

On Lie Group IMU and Linear Velocity Preintegration for Autonomous Navigation Considering the Earth Rotation Compensation

Pau Vial ^{1b}, Joan Solà ^{1b}, Narcís Palomeras ^{1b}, and Marc Carreras ^{1b}, *Member, IEEE*

Abstract—Robot localization is a fundamental task in achieving true autonomy. Recently, many graph-based navigators have been proposed that combine an inertial measurement unit (IMU) with an exteroceptive sensor applying IMU preintegration to synchronize both sensors. IMUs are affected by biases that also have to be estimated. To increase the navigator robustness when faults appear on the perception system, IMU preintegration can be complemented with linear velocity measurements obtained from visual odometry, leg odometry, or a Doppler Velocity Log (DVL), depending on the robotic application. Moreover, higher grade IMUs are sensitive to the Earth rotation rate, which must be compensated in the preintegrated measurements. In this article, we propose a general purpose preintegration methodology formulated on a compact Lie group to set motion constraints on graph simultaneous localization and mapping problems considering the Earth rotation effect. We introduce the $SE_N(3)$ group to jointly preintegrate IMU data and linear velocity measurements to preserve all the existing correlation within the preintegrated quantity. Field experiments using an autonomous underwater vehicle equipped with a DVL and a navigational grade IMU are provided and results are benchmarked against a commercial filter-based inertial navigation system to prove the effectiveness of our methodology.

Index Terms—Autonomous vehicle navigation, kinematics, lie theory, marine robotics.

I. INTRODUCTION

INERTIAL Measurement Unit (IMU) preintegration consists on the aggregation of several consecutive IMU measurements into a single pseudomeasurement representing the relative motion of the sensor during this interval. In the last years, IMU preintegration has been applied to several Graph simultaneous

Received 4 October 2024; revised 29 November 2024; accepted 6 December 2024. Date of publication 24 December 2024; date of current version 12 February 2025. The work of Pau Vial was supported by the PhD under Grant FPU19/03638. This work was supported in part by the BITER-AUV Project under Grant PID2020-114732RB-C33, in part by the PLOME Project under Grant PLEC2021-007525, in part by the EBCON Project under Grant PID2020119244GB-I00, and in part by the Consolidated Research Group RAIG under Grant 2021 SGR 00510 of the Departament de Recerca i Universitats de la Generalitat de Catalunya. Open Access funding was provided thanks to the CRUE-CSIC agreement with IEEE. This article was recommended for publication by Associate Editor A. Nuechter and Editor S. Behnke upon evaluation of the reviewers' comments. (*Corresponding author: Pau Vial.*)

Pau Vial, Narcís Palomeras, and Marc Carreras are with the Institut VICOROB, Universitat de Girona, 17003 Girona, Catalunya, Spain (e-mail: pau.vial@udg.edu).

Joan Solà is with the Institut de Robòtica i Informàtica Industrial (IRII), CSIC-Universitat Politècnica de Catalunya, 08028 Barcelona, Catalunya, Spain.

Digital Object Identifier 10.1109/TRO.2024.3521865

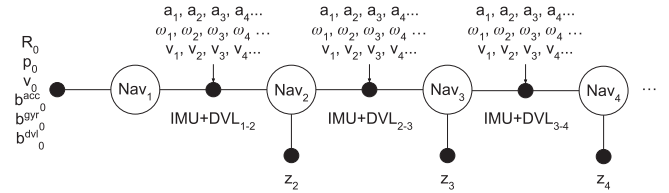


Fig. 1. Factor graph applying the joint IMU and DVL preintegration factor and the depth prior z to set a graph-based INS. A robot state $Nav_i \in \langle SE_2(3), \mathbb{R}^3, \mathbb{R}^3, \mathbb{R}^3 \rangle$ is formed by the robot orientation $R \in SO(3)$, position $p \in \mathbb{R}^3$ and linear velocity $v \in \mathbb{R}^3$ and the sensors bias b^{acc} , b^{gyr} , $b^{dvl} \in \mathbb{R}^3$.



Fig. 2. Girona 1000 AUV from IQUA Robotics. (a) General view and (b) robot deployment at sea using the Sextant boat from Universitat de Girona.

localization and mapping (SLAM) problems [1] to synchronize an exteroceptive sensor with an IMU. By using IMU preintegration, we avoid to set a node for each IMU measurement, which involves handling very massive graphs since an IMU typically runs at hundreds of Hertz. Thus, IMU measurements are preintegrated between relevant exteroceptive measurements, that normally are received in a much lower frequency, to set only a graph node when a key frame is processed, significantly mitigating the graph growth. IMU preintegration was first proposed to build a graph-based visual-inertial navigation system (VINS) [2], where an IMU and an optical camera were fused in a Graph Simultaneous Localization and Mapping (Graph SLAM) problem. Through this methodology, a node to the graph was only set every time a frame of the camera was processed and all IMU measurements between key frames were accumulated into a single motion constraint. Many graph-based navigators apply this principle. For instance, other Visual-Inertial Navigation System (VINS) are [3], [4] and an IMU can also be combined with a

LiDAR to build a LiDAR-inertial navigation system (LINS) [5] or with Global Navigation Satellite System (GNSS) measurements to build an inertial navigation system (INS) [6]. Finally, more sensors can be fused to build more complex navigators, such as a LiDAR-VINS (LVINS) [7], [8], combining a LiDAR with an optical camera, or a Visual-Inertial-Magnetic Navigation System (VIMNS) [9], combining a magnetometer with an optical camera.

IMUs are classified in four accuracy grades depending on the technology applied to build the device: consumer, industrial, tactical, and navigational. Lower grade IMUs are based on Micro-ElectroMechanical Systems (MEMS) that can measure both linear acceleration and angular rate depending on the movement of suspended masses. This kind of device has a very competitive accuracy-cost rate. However, the sensor biases grow fast, degenerating the pose integration in a few seconds. Higher grade IMUs are typically based on the combination of MEMS-based accelerometers with Fibre-Optic Gyroscopes (FOG). FOGs are high precision gyroscopes that measure the angular rate of a moving body based on the phase shift experienced by photons that travel at opposite directions through a fiber optic coil due to the Sagnac effect. Through this technology, high grades of precision are obtained, giving rise to devices sensitive to the Earth rotation rate ($15^\circ/\text{h}$). Therefore, when high grade IMUs are preintegrated, the Earth rotation rate has to be removed from the FOG measurements, as in common accelerometers, where measurements are compensated from gravity. New MEMS-based IMU designs can also reach tactical precision grades by setting a multi-IMU array equipped with several MEMS IMUs in a compact device. It has been proved that this kind of sensor can also be sensitive to the Earth rotation effect [10], [11]. Therefore, compensating for the perturbation caused by the Earth's rotation when preintegrating a higher grade IMU is crucial to reduce the drift of the estimation.

Usually preintegration only applies to IMUs, where gyroscopes are integrated to obtain robot orientation and accelerometers are double integrated to obtain robot position. However, the double integration of accelerometers produces significant positional error, specially if lower grade accelerometers that rapidly accumulate bias are used. To improve the accuracy of a preintegrated measurement, an IMU can jointly be preintegrated with a Linear Velocity Sensor (LVS). As linear velocity is only integrated once, the robot position estimation can be improved and linear velocity measurements can help to better estimate the accelerometers bias. This preintegration approach was first proposed for a legged robot [7], where the linear velocity of the robot was extracted from the leg kinematics and it was preintegrated with the IMU measurements building a Graph SLAM problem combining optical and LiDAR information. However, other methodologies to measure the robot linear velocity are available for other robot typologies, such as the use of a Doppler Velocity Log (DVL) in underwater robotics involving an Autonomous Underwater Vehicles (AUVs) or visual odometry extracted from optical cameras or event cameras [12], [13] mounted on autonomous aerial vehicles (AAVs) or ground robots. Therefore, complementing IMU preintegration with linear velocity measurements is an interesting approach to improve

the preintegrated measurements accuracy, especially during exteroceptive data outages to maintain an acceptable estimation of the IMU bias.

An important aspect to consider when jointly preintegrating an IMU and an LVS is the correlation that appears between the obtained preintegrated quantities. Although we are considering two sensors providing independent measurements, the obtained preintegrated IMU and LVS positions are correlated through the preintegrated orientation as both quantities are built sharing the same gyroscopes measurements. This fact, consisting in the appearance of an unexpected correlation between preintegrated measurements built using independent measurements, was first observed in legged robotics. In that case, the IMU preintegration was combined with joints preintegration considering centroidal dynamics and a correlation was observed between the estimated forces and the measured linear acceleration [14], [15, Chap. 7]. Thus, when such a correlation appears, the sensors have to be preintegrated in a single measurement for two main reasons. First, to naturally find all the correlation existing between the quantities to define a tightly coupled estimation problem. Second, to not break the independence between factors imposed by the Graph SLAM problem definition that allows to factorize the problem joint probability distribution into small probability distributions or factors. However, to the best of the authors' knowledge, no published IMU and LVS preintegration methodology jointly preintegrates both sensors in a single compact group.

In this article, we present a general purpose methodology to preintegrate IMU and LVS measurements and to evaluate its residuals in a single compact group to solve a Graph SLAM problem. The key features of this methodology are as follows:

- 1) The combination of IMU measurements with linear velocity measurements to increase the estimator accuracy.
- 2) The compensation of the perturbation caused by the Earth's rotation measured by higher grade IMUs.

To do it we introduce the $\text{SEN}_N(3)$ group, which is a generalization of the $\text{SE}(3)$ group, and we analyze three different sensors configurations: (i) gyroscopes and LVS, (ii) IMU-only, and (iii) IMU and LVS; being (iii) the main contribution of this article. Working at the $\text{SEN}_N(3)$ group allows to:

- 1) define a general and rigorous formulation for all the analyzed cases considering Lie groups;
- 2) jointly preintegrate all the measurements in a single factor preserving all the existing correlation and ensuring a tightly coupled estimator.

In addition, all the required jacobians are provided in analytic form in the $\text{SEN}_N(3)$ group with their proofs. Field experiments are performed to test the proposed methodology concretized on an AUV equipped with a navigational grade IMU, sensitive to the Earth rotation rate, and a DVL used as the LVS. The experimentation was performed in the absence of exteroceptive measurements to prove the robustness of the system, showing how the navigator can manage perception outages of at least 1 h long when applying the joint IMU and LVS preintegration and considering the Earth rotation compensation.

The rest of this article is organized as follows. Section II summarizes the state of the art. Section III defines the considered

robotic system and Section IV reviews the preintegration theory formulated on Lie groups. To do it, we follow the notation and terminology for Lie theory used by Solà et al. [16]. In Section V the methodology to compute preintegrated measurements is presented, whereas preintegration residuals are provided in Section VI. Finally, the proposed methodology is tested on field experiments. Section VII describes the experimental setup, Section VIII presents the results, which are discussed in Sections IX. Finally, Section X concludes this article.

II. STATE OF THE ART

IMU preintegration was first proposed by Lupton et al. [2], [17] to build a graph-based VINS, where the IMU kinematic model was formulated using Euler angles. In this preliminary work, Lupton already introduced the first-order Taylor approximation of the preintegrated measurements on the sensor biases that is commonly used to update the preintegrated measurement when a better estimation for the biases is available. The methodology proposed by Lupton was also used by Indelman et al. [18] to build a graph-based navigator fusing IMU, GNSS, and stereo camera measurements. Forster et al. [3], [19] proposed another graph-based VINS introducing Lie theory [16] to propagate the IMU preintegrated uncertainty formulating the IMU kinematic model at the $\langle \text{SO}(3) \times T(3), \mathbb{R}^3 \rangle$ composite manifold, where $\text{SO}(3) \times T(3)$ parameterizes the robot pose and \mathbb{R}^3 represents the robot linear velocity. Forster et al. made his IMU preintegration implementation available in the GTSAM library [20], and it is the standard open-source implementation nowadays. The IMU kinematic model applied by Forster et al. is a discrete-time model, corresponding to an approximation of the real continuous-time model. On the contrary, Ekenhoff et al. [21], [22] proposed two continuous models, where IMU measurements and error dynamics are analytically preintegrated in a continuous-time fashion, defining the piecewise constant measurements model (PCMM) and the piecewise constant local true acceleration model, in contrast to the discrete-time model applied by Forster that they call the constant global acceleration model (CGAM). Finally, Brossard et al. [23], [24] proposed a new preintegration methodology, formulating the IMU kinematic model at the $\text{SE}_2(3)$ group, supporting the continuous-time Piecewise Constant Measurements Model (PCMM) and the discrete-time Constant Global Acceleration Model (CGAM). By applying Monte-Carlo simulations, they demonstrated that the $\text{SE}_2(3)$ group is the proper Lie group to model the IMU preintegration uncertainty, obtaining a probabilistic dispersion that resembles the expected “banana” shape more than the standard Gaussian ellipse obtained by applying the $\langle \text{SO}(3) \times T(3), \mathbb{R}^3 \rangle$ composite manifold.

Another important contribution of the work of Brossard et al. is the introduction of the Earth rotation compensation on the IMU kinematic model to be able to preintegrate higher grade IMUs. By applying this methodology, they could remove the Earth rotation rate perturbation on the gyroscope measurements and the centrifugal and Coriolis accelerations caused by the Earth rotation rate on the accelerometer measurements, showing better pose accuracy on the estimation. Tang et al. [25]

proposed a similar methodology to compensate the Earth rotation effect, but they formulated the IMU kinematic model at the $\langle S^3 \times T(3), \mathbb{R}^3 \rangle$ composite manifold, using quaternions instead of the $\text{SO}(3)$ group. In the results, they demonstrated that the Earth rotation compensation is also necessary for higher grade MEMS-based IMUs, proving that these devices are also sensitive to the Earth rotation effects. Jiang et al. [26] applied a similar IMU kinematic model, where the Earth rotation and the gravity change through the robot geodetic position was considered for long term operation covering huge areas, a feature already considered for most filter-based Inertial Navigation Systems (INS). Moreover, in his algorithm, Jiang propagates the preintegration uncertainty in the square root information matrix form in order to have better numerical stability. Zhang et al. [27] proposed a more accurate IMU kinematic model than that applied at [24] and [25], which improves the estimation accuracy for vehicles submitted to huge dynamics at high speed. However, the model was formulated at the $\langle \text{SO}(3) \times T(3), \mathbb{R}^3 \rangle$ composite manifold, not correctly representing the preintegrated uncertainty. They tested their algorithm using a FOG-based IMU and showed that their IMU model outperforms filtered-based INS. Finally, Ding et al. [28] proposed the equivalent rotation vector model to compensate Earth rotation, propagating uncertainty on the $\langle \text{SO}(3) \times T(3), \mathbb{R}^3 \rangle$ composite manifold.

In order to improve the navigator accuracy when faults appear on the exteroceptive sensor, Chang et al. [29] extended the IMU preintegrated measurement with car odometer measurements, preintegrating together the vehicle kinematic model with the IMU kinematic model, considering the CGAM defined at the $\langle S^3 \times T(3), \mathbb{R}^3 \rangle$ composite manifold using quaternions. By applying this methodology, they built a car navigator, fusing preintegrated measurements with GNSS and LiDAR observations. Bai et al. [30] applied a similar approach to build a graph-based navigator applying GNSS measurements. Their results show how by applying this coupled preintegrated measurement, the estimation accuracy improves in the presence of GNSS outages in comparison to filters. In a different approach to improve the preintegration accuracy, Wisth et al. [7] combined IMU preintegration with linear velocity preintegration using velocity measurements obtained from leg odometry. To do this, they considered two different factors: a preintegrated IMU factor considering the CGAM [3] and a new preintegrated factor considering a constant velocity model defined at the $\text{SO}(3) \times T(3)$ group aggregating the gyroscopes and the LVS measurements. As the preintegrated orientation was computed at both factors, they needed to impose a constraint to the problem to only consider it once. However, by applying two different factors that share the same gyroscopes measurements, they break the factors independence constraint imposed at the Graph SLAM problem definition, as both preintegrated quantities are correlated. The same preintegration methodology was applied by Thoms et al. [8] on a navigation problem implying a surface marine vehicle that used a DVL as the LVS. Finally, novel approaches increase the navigator robustness by substituting the typical Brownian motion modeling IMU bias dynamics for a neural network that learns the IMU bias evolution during perception outages [31] or

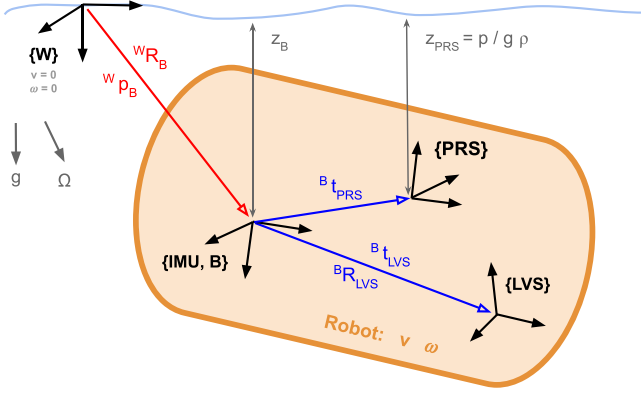


Fig. 3. Robot with sensors rigidly attached. The IMU is on the body frame $\{B\}$ and the LVS and the pressure sensor have their own frames. The robot is moving relative to an inertial reference frame $\{W\}$ with time-varying velocity v and angular rate ω . Gravity g and Earth rotation Ω are constant at $\{W\}$.

by using Gaussian Processes to learn the IMU dynamics avoiding imposing any kinematic model and performing a continuous analytical preintegration [32].

In this article, we propose a preintegration methodology that 1) jointly preintegrates IMU and LVS measurements to improve the navigator robustness in the presence of exteroceptive sensor faults; 2) defines the preintegration model at a compact group to properly propagate the preintegrated measurement uncertainty; and 3) compensates the Earth rotation to properly use higher grade IMUs. To the best of the authors' knowledge, no methodology exists combining these three key features.

III. ROBOTIC SYSTEM DESCRIPTION

We assume a mobile robot equipped with an IMU, providing robot linear acceleration a and angular rate ω ; an LVS, measuring robot linear velocity v ; and a pressure sensor, providing absolute height or depth ${}^W z$. As shown in Fig. 3, we set the robot base link $\{B\}$ at the IMU reference frame and we consider that the pressure sensor and the LVS may not be assembled at the base link of the robot, being ${}^B R_{LVS}$ and ${}^B t_{LVS}$ the orientation and the position of the LVS at the body frame and ${}^B t_{PRS}$ the position of the pressure sensor at the body frame. Since depth is derived from pressure, which is an absolute measurement in the global frame, there is no need to consider any orientation of the pressure sensor.

The whole system shown in Fig. 3 is referenced to an inertial reference frame called world $\{W\}$, where the robot position and orientation are, respectively, modeled by ${}^W p_B$ and ${}^W R_B$. The world frame is considered a North East Down (NED) system placed on the Earth surface, defined by a latitude ϕ_0 and a longitude λ_0 . At this reference frame, the gravity g and the Earth rotation Ω vectors are modeled as follows:

$$\begin{aligned} g &= \begin{bmatrix} 0 & 0 & g \end{bmatrix}^T, \\ \Omega &= \omega_E \begin{bmatrix} \cos \phi_0 & 0 & -\sin \phi_0 \end{bmatrix}^T, \end{aligned} \quad (1)$$

TABLE I
GLOBAL ACTIONS ACTING ON THE ROBOT

Property	Symbol	Magnitude
Gravity acceleration	g	9.81 m/s
Earth rotation rate	ω_E	15 °/h
Mediterranean sea water density	ρ	1030 kg/m ³

where g is the gravity acceleration and ω_E is the Earth rotation rate. In this article, we consider the common accepted approximations at the Mediterranean coast given in Table I.

For the sensors observation model, we assume that all measurements (linear acceleration \bar{a} , angular rate $\bar{\omega}$ and linear velocity \bar{v}) are affected by a Gaussian white noise and accelerometers, gyroscopes and the LVS are biased

$$\begin{aligned} a &= \bar{a} - b^{\text{acc}} + \eta^{\text{acc}} & \text{with } \eta^{\text{acc}} &\sim \mathcal{N}(0_{3 \times 1}, Q^{\text{acc}}), \\ \omega &= \bar{\omega} - b^{\text{gyr}} + \eta^{\text{gyr}} & \text{with } \eta^{\text{gyr}} &\sim \mathcal{N}(0_{3 \times 1}, Q^{\text{gyr}}), \\ v &= \bar{v} - b^{\text{lvs}} + \eta^{\text{lvs}} & \text{with } \eta^{\text{lvs}} &\sim \mathcal{N}(0_{3 \times 1}, Q^{\text{lvs}}), \end{aligned} \quad (2)$$

where all biases b are modeled by a Brownian motion as they are slow time-varying quantities

$$\begin{aligned} b_{k+1}^{\text{acc}} &= b_k^{\text{acc}} + \eta^{\text{ba}} & \text{with } \eta^{\text{ba}} &\sim \mathcal{N}(0_{3 \times 1}, Q^{\text{ba}}), \\ b_{k+1}^{\text{gyr}} &= b_k^{\text{gyr}} + \eta^{\text{bg}} & \text{with } \eta^{\text{bg}} &\sim \mathcal{N}(0_{3 \times 1}, Q^{\text{bg}}), \\ b_{k+1}^{\text{lvs}} &= b_k^{\text{lvs}} + \eta^{\text{bv}} & \text{with } \eta^{\text{bv}} &\sim \mathcal{N}(0_{3 \times 1}, Q^{\text{bv}}). \end{aligned} \quad (3)$$

Considering that the LVS is rigidly attached to the robot, both systems form a rigid body that is in rototranslation. Since the LVS is measuring the robot linear velocity at its own frame ${}^{\text{LVS}} v$, this measurement can be mapped to the body frame by applying screw theory

$${}^B v = {}^B R_{LVS} {}^{\text{LVS}} v + [{}^B t_{LVS}]_{\times} {}^B \omega \quad (4)$$

where ${}^B \omega$ is the angular velocity of the vehicle measured by the IMU gyroscopes (placed at the robot base link). Since the robot is in motion in reference to an inertial reference frame $\{W\}$, the robot linear velocity measured at the body frame can be mapped to the world frame by applying

$${}^W v = {}^W R_B {}^B v \quad (5)$$

where ${}^B v$ is defined at (4). Considering the sensors observation model, substituting (2) into (5), the observation model for the robot linear velocity at the world frame is

$$\begin{aligned} {}^W v &= {}^W R_B \left({}^B R_{LVS} (\bar{v} - b^{\text{lvs}} \right. \\ &\quad \left. + \eta^{\text{lvs}}) + [{}^B t_{LVS}]_{\times} \left(\bar{\omega} - b^{\text{gyr}} + \eta^{\text{gyr}} \right) \right). \end{aligned} \quad (6)$$

IV. PREINTEGRATION PRELIMINARIES

In Graph SLAM problems preintegration allows the combination of many measurements between two key frames into a single relative motion constraint. In this section, we introduce a general model for preintegration considering Lie Groups. To

do so, first, we present a generalization of the Special Euclidean group SE(3) (SE(3)) group where this model is formulated.

A. The $SE_N(3)$ Group

The $SE_N(3)$ group [33], [34] is the Lie Group [16] of N isometries jointly encoding a rotation matrix $R \in SO(3)$ with N vectors $u_i \in \mathbb{R}^3$. Using homogeneous matrices, the $SE_N(3)$ group can be algebraically expressed as

$$SE_N(3) := \left\{ T = \begin{bmatrix} R & | & u_1 & \dots & u_N \\ \hline 0_{N \times 3} & | & I_N & & \end{bmatrix} \in \mathbb{R}^{(3+N) \times (3+N)} \left| \begin{array}{l} R \in SO(3) \\ u_i \in \mathbb{R}^3 \end{array} \right. \right\}$$

where matrix multiplication provides composition and matrix inverse gives the inverse element, having the closed form

$$T^{-1} = \begin{bmatrix} R^T & | & -R^T u_1 & \dots & -R^T u_N \\ \hline 0_{N \times 3} & | & I_N & & \end{bmatrix}. \quad (7)$$

The group tangent space is $\varepsilon = [\phi^T \ \nu_1^T \ \dots \ \nu_N^T]^T \in \mathbb{R}^{3N+3}$, where $\phi \in \mathbb{R}^3$ encodes orientation and $\nu_i \in \mathbb{R}^3$. To transform elements from the tangent space to the manifold and vice-versa, the exponential map and the logarithm map are

$$\text{Exp}(\varepsilon) = \begin{bmatrix} \exp(\phi) & | & J_l(\phi)\nu_1 & \dots & J_l(\phi)\nu_N \\ \hline 0_{N \times 3} & | & I_N & & \end{bmatrix},$$

$$\text{Log}(T) = \begin{bmatrix} \log(R) \\ J_l^{-1}(\log(R))u_i \\ \vdots \\ J_l^{-1}(\log(R))u_N \end{bmatrix}, \quad (8)$$

where $\exp(\phi)$, $\log(R)$, and $J_l(\phi)$ are the exponential map, the logarithm map, and the left jacobian of the Special Orthogonal group SO(3) group (see [16, Appendix B]). Using these operators, the right-handed addition and subtraction at the group are defined as

$$T_2 = T_1 \oplus \varepsilon \triangleq T_1 \cdot \text{Exp}(\varepsilon),$$

$$\varepsilon = T_2 \ominus T_1 \triangleq \text{Log}(T_1^{-1} \cdot T_2), \quad (9)$$

where $T_1, T_2 \in SE_N(3)$ and ε is a perturbation at the tangent space of $SE_N(3)$. To map a vector tangent to the point $T \in SE_N(3)$ to a vector tangent to the Identity, the adjoint map is

$$\text{Ad}(T) = \begin{bmatrix} R & 0_3 & \dots & 0_3 \\ [u_1]_{\times} R & R & \dots & 0_3 \\ \vdots & \vdots & \ddots & \vdots \\ [u_N]_{\times} R & 0_3 & \dots & R \end{bmatrix} \in \mathbb{R}^{(3N+3) \times (3N+3)} \quad (10)$$

where $[\]_{\times}$ is the hat operator converting an \mathbb{R}^3 vector into a skew symmetric matrix $\mathbb{R}^{3 \times 3}$. The right jacobian of the group, corresponding to the derivative of the exponential map, is

$$J_r(T) = \begin{bmatrix} J_r(\phi) & 0_3 & \dots & 0_3 \\ Q_{\phi, \nu_1} & J_r(\phi) & \dots & 0_3 \\ \vdots & \vdots & \ddots & \vdots \\ Q_{\phi, \nu_N} & 0_3 & \dots & J_r(\phi) \end{bmatrix} \in \mathbb{R}^{(3N+3) \times (3N+3)} \quad (11)$$

where $J_r(\phi)$ is the right jacobian of the SO(3) group and

$$Q_{\phi, \nu} = \frac{1}{2} \nu_{\times} + \frac{\phi - \sin \phi}{\phi^3} (\phi_{\times} \nu_{\times} + \nu_{\times} \phi_{\times} + \phi_{\times} \nu_{\times} \phi_{\times})$$

$$+ \frac{\phi^2 + 2 \cos \phi - 2}{\phi^4} (\phi_{\times}^2 \nu_{\times} + \nu_{\times} \phi_{\times}^2 - 3 \phi_{\times} \nu_{\times} \phi_{\times})$$

$$+ \frac{2\phi - 3 \sin \phi + \phi \cos \phi}{\phi^5} (\phi_{\times} \nu_{\times} \phi_{\times}^2 + \phi_{\times}^2 \nu_{\times} \phi_{\times}).$$

B. Preintegration on Lie Groups

In the context of Graph SLAM, the preintegrated measurement Υ_k between two consecutive keyframes $T_k, T_{k+1} \in SE_N(3)$ is related by [24]

$$T_{k+1} = \Gamma_k \cdot \Phi(T_k, \tau) \cdot \Upsilon_k \quad (12)$$

where $\Gamma, \Upsilon \in SE_N(3)$ are elements of the same Lie Group as T and $\Phi : SE_N(3), \mathbb{R} \rightarrow SE_N(3)$ is an automorphism that integrates T through the sampling time τ of the sensor, as the robotic system kinematics defines a group affine system [24], [35]. Analyzing the composition defined by (12), Γ is an element encoding global actions on T_k , whereas Υ encodes local actions on T_k . In the context of robotics where T_k is modeling robot motion, Γ encodes motion modeled at the world frame, whereas Υ encodes motion modeled at the body frame. This differentiation between global and local actions simplifies how to model the preintegration problem.

Preintegration consists of the accumulation of measurements between two key frames. As proprioceptive sensors are mounted on a robot, their measurements are referenced on the local frame of the robot. Therefore, the measurements preintegration can be modeled by the element Υ . However, precise inertial sensors not only measure robot motion, but also the gravity acceleration or the Earth rotation rate, which are constant actions at the world frame. Thus, preintegrated measurements at Υ are perturbed by global actions that have to be compensated in order to estimate the robot navigation. As the necessary compensation is caused by constant global actions, it is easier to model them on the Γ element than to convert global actions to local actions to compensate directly the measurements before preintegrating, as this is done when filtering. Therefore, by applying the preintegration scheme of (12), Υ models measurements preintegration and Γ models gravity and Earth rotation compensation. If only the gravity compensation is considered, the IMU kinematic model is called the Flat Earth Model (FEM); whereas if both gravity and Earth rotation are compensated, the Rotating Earth Model (REM) is defined. In this article, Γ will be provided in Section VI for each of these models, whereas Υ will be defined for each of the analyzed sensors configurations in Section V.

When facing a Graph SLAM problem, two actions are required: preintegration of measurements while acquiring data and computation of residuals to solve the problem. During preintegration, the element Υ_{ij} is calculated by directly accumulating the raw measurements without applying any type of compensation. This element can be updated incrementally while

receiving data by applying [24]

$$\Upsilon_{ij} = \prod_{k=1}^{j-1} \Phi(\Upsilon_k, (j-1-k)\tau) \quad (13)$$

where τ is the sampling time of the sensors. Note that this series depends on the total preintegration time as j appears inside the series. Thus, the final moment of preintegration needs to be known a priori before starting to accumulate measurements. On solving the graph, residuals are evaluated and the accumulated measurements are compensated from global actions. The preintegration residual between key frames T_j and T_i is found by inverting (12) reaching

$$r_{ij} = \Sigma_{ij}^{-1/2} \left((\Phi(T_i, \Delta t)^{-1} \cdot \Gamma_{ij}^{-1} \cdot T_j) \ominus \Upsilon_{ij} \right) \quad (14)$$

where Δt is the elapsed time while preintegrating Υ_{ij} and Σ_{ij} is the covariance matrix associated to Υ_{ij} .

V. ON-MANIFOLD PREINTEGRATION

By applying the preintegration model of (12), raw proprioceptive measurements can be accumulated on a preintegrated measurement Υ_{ij} . In the following sections, the methodology to obtain the preintegrated measurement expectation and uncertainty for different sensors configurations is presented.

A. Joint Gyroscopes and Linear Velocity Sensor Preintegration

The combination of three gyroscopes with an LVS usually is applied to robots with slow dynamics, as a constant velocity model is assumed. For this configuration, linear velocities and angular rates are integrated at the SE(3) group

$$\text{SE}_1(3) = \left\{ T = \begin{bmatrix} R & p \\ 0_{1 \times 3} & 1 \end{bmatrix} \in \mathbb{R}^{4 \times 4} \mid \begin{array}{l} R \in \text{SO}(3) \\ p \in \mathbb{R}^3 \end{array} \right\}$$

where R and p , respectively, model the robot orientation and position and the group tangent space is $\varepsilon = [\phi^T, \rho^T]^T \in \mathbb{R}^6$. Considering that gyroscopes and the LVS may not be assembled at the same place on the robot, in comparison to an IMU, where accelerometers and gyroscopes are referenced to the same frame, the observation model of (4) must be applied. By combining this observation model with a constant velocity kinematic model, measurements are exponentiated to the SE(3) group as

$$\Upsilon_k^{\text{lvs}} = \left[\begin{array}{c|c} \exp(\omega_k \tau) & \tau ({}^B R_{\text{LVS}} v_k + [{}^B t_{\text{LVS}}] \times \omega_k) \\ \hline 0_{1 \times 3} & 1 \end{array} \right] \quad (15)$$

where v_k and ω_k follow the observation model of (2).

Considering a first order Taylor expansion, SO(3) jacobians relate small perturbations at the tangent space of SO(3) by $\exp(\phi + \delta\phi) \approx \exp(\phi) \exp(J_r(\phi)\delta\phi)$. Applying this identity on the rotational part of (15), Υ_k^{lvs} can be factorized into two factors

$$\Upsilon_k^{\text{lvs}} \approx \bar{\Upsilon}_k^{\text{lvs}} \cdot \text{Exp} \left(G_k^{\text{lvs}} \begin{bmatrix} \eta^{\text{gyr}} \\ \eta^{\text{lvs}} \end{bmatrix} \right) \quad (16)$$

where

$$\bar{\Upsilon}_k^{\text{lvs}} = \left[\begin{array}{c|c} \exp(\hat{\omega}_k \tau) & \tau ({}^B R_{\text{LVS}} \hat{v}_k + [{}^B t_{\text{LVS}}] \times \hat{\omega}_k) \\ \hline 0_{1 \times 3} & 1 \end{array} \right],$$

$$G_k^{\text{lvs}} = \begin{bmatrix} \tau J_r(\hat{\omega}_k \tau) & 0_3 \\ \tau \exp(\hat{\omega}_k \tau)^T [{}^B t_{\text{LVS}}]_{\times} & \tau \exp(\hat{\omega}_k \tau)^T {}^B R_{\text{LVS}} \end{bmatrix},$$

being $\bar{\Upsilon}_k^{\text{lvs}}$ a noise agnostic factor that can be evaluated using the sensor data, $\hat{\omega}_k = \bar{\omega}_k - b^{\text{gyr}}$ and $\hat{v}_k = \bar{v}_k - b^{\text{lvs}}$.

To incrementally compute the preintegrated measurement $\bar{\Upsilon}_{ij}^{\text{lvs}}$ while receiving measurements, we apply (13). Considering that at the SE(3) group $\Phi_{\text{SE}(3)}(T, \tau) = T$, (13) simplifies to the following incremental form:

$$\bar{\Upsilon}_{i(j+1)}^{\text{lvs}} = \bar{\Upsilon}_{ij}^{\text{lvs}} \cdot \bar{\Upsilon}_j^{\text{lvs}} \quad (17)$$

that do not depend on the final preintegration time. To compute the covariance matrix Σ_{ij}^{lvs} related to the preintegrated measurement $\bar{\Upsilon}_{ij}^{\text{lvs}}$, we perform uncertainty propagation on (17) by applying a first-order Taylor expansion. Taking derivatives on (17), we can update Σ_{ij}^{lvs} while preintegrating applying

$$\Sigma_{i(j+1)}^{\text{lvs}} = A_j^{\text{lvs}} \Sigma_{ij}^{\text{lvs}} A_j^{\text{lvs}T} + B_j^{\text{lvs}} G_j^{\text{lvs}} \begin{bmatrix} Q^{\text{gyr}} & 0_3 \\ 0_3 & Q^{\text{lvs}} \end{bmatrix} G_j^{\text{lvs}T} B_j^{\text{lvs}T} \quad (18)$$

starting from the initial condition $\Sigma_{ii}^{\text{lvs}} = 0_{6 \times 6}$ where

$$A_j^{\text{lvs}} = \frac{\partial \bar{\Upsilon}_{i(j+1)}}{\partial \bar{\Upsilon}_{ij}} = \frac{\partial \bar{\Upsilon}_{ij} \cdot \bar{\Upsilon}_j}{\partial \bar{\Upsilon}_{ij}} = \text{Ad} \left(\bar{\Upsilon}_j^{\text{lvs}^{-1}} \right),$$

$$B_j^{\text{lvs}} = \frac{\partial \bar{\Upsilon}_{i(j+1)}}{\partial \bar{\Upsilon}_j} = \frac{\partial \bar{\Upsilon}_{ij} \cdot \bar{\Upsilon}_j}{\partial \bar{\Upsilon}_j} = I_6$$

and Q models sensors noise defined in (2).

For this configuration, if a null measurement is received, the robot remains static in position, as in (15) a constant velocity model is considered. Therefore, no position compensation is needed to the Γ element of (12) and the only possible compensation is for the rotational part. Thus, at the SE(3) group the compensation factor has the following form:

$$\Gamma^{\text{lvs}} = \left[\begin{array}{c|c} \Gamma_R & 0_{3 \times 1} \\ \hline 0_{1 \times 3} & 1 \end{array} \right] \quad (19)$$

where Γ_R will be defined later in Section VI for the FEM and the REM.

B. Joint Gyroscopes and Accelerometers (IMU) Preintegration

An IMU is a sensor widely applied on robotics, having the accelerometers and the gyroscopes referenced at the same frame. When this sensor is considered, linear accelerations and angular rates are integrated at the SE₂(3) group [24]

$$\text{SE}_2(3) := \left\{ T = \begin{bmatrix} R & p & v \\ 0_{2 \times 3} & I_2 \end{bmatrix} \in \mathbb{R}^{5 \times 5} \mid \begin{array}{l} R \in \text{SO}(3) \\ p, v \in \mathbb{R}^3 \end{array} \right\}$$

where R , p , and v , respectively, model the robot orientation, position and linear velocity measured at world frame and the group tangent space is $\varepsilon = [\phi^T, \rho^T, \nu^T]^T \in \mathbb{R}^9$. Robot linear velocity needs to be represented in the group as it is the intermediate state between the measured linear acceleration and the estimated position. Considering the CGAM by assuming a vehicle with slow dynamics where the acceleration vector is dominated by

the gravity, measurements are retracted to the $SE_2(3)$ group by the following simplified exponential [22]:

$$\Upsilon_k^{\text{imu}} = \left[\begin{array}{c|c|c} \exp(\omega_k \tau) & \frac{\tau^2}{2} a_k & \tau a_k \\ \hline 0_{2 \times 3} & I_2 & \end{array} \right] \quad (20)$$

where a_k and ω_k follow the observation model of (2). Following a similar development to that of (16), Υ_k^{imu} can be factorized into two factors

$$\Upsilon_k^{\text{imu}} \approx \bar{\Upsilon}_k^{\text{imu}} \cdot \text{Exp} \left(G_k^{\text{imu}} \begin{bmatrix} \eta^{\text{acc}} \\ \eta^{\text{gyr}} \end{bmatrix} \right) \quad (21)$$

where

$$\bar{\Upsilon}_k^{\text{imu}} = \left[\begin{array}{c|c|c} \exp(\hat{\omega}_k \tau) & \frac{\tau^2}{2} \hat{a}_k & \tau \hat{a}_k \\ \hline 0_{2 \times 3} & I_2 & \end{array} \right],$$

$$G_k^{\text{imu}} = \begin{bmatrix} 0_3 & \tau J_\tau(\hat{\omega}_k \tau) \\ \frac{\tau^2}{2} \exp(\hat{\omega}_k \tau)^T & 0_3 \\ \tau \exp(\hat{\omega}_k \tau)^T & 0_3 \end{bmatrix},$$

being $\bar{\Upsilon}_k^{\text{imu}}$ a noise agnostic factor, $\hat{a}_k = \bar{a}_k - b^{\text{acc}}$ and $\hat{\omega}_k = \bar{\omega}_k - b^{\text{gyr}}$.

To incrementally compute the preintegrated measurement $\bar{\Upsilon}_{ij}^{\text{imu}}$ following (13), first, we need to consider the identity provided in Lemma 1 that can be easily proved.

Lemma 1: Given two poses $T_1, T_2 \in SE_N(3)$ and the automorphism $\Phi : SE_N(3), \mathbb{R} \rightarrow SE_N(3)$ defined at Proposition 1 and 2, then

$$\Phi(\Phi(T_1, \tau_1) \cdot T_2, \tau_2) = \Phi(\Phi(T_1, \tau_1), \tau_2) \cdot \Phi(T_2, \tau_2).$$

Thus, using the definition of $\Phi_{SE_2(3)}(T, \tau)$ given by Proposition 1 provided in the Appendix and applying Lemma 1, (13) results in

$$\bar{\Upsilon}_{i(j+1)}^{\text{imu}} = \Phi_{SE_2(3)}(\bar{\Upsilon}_{ij}^{\text{imu}}, \tau) \cdot \bar{\Upsilon}_j^{\text{imu}} \quad (22)$$

which again is an incremental series that does not depend on the final preintegrated state. To compute the covariance matrix Σ_{ij}^{imu} related to the preintegrated measurement $\bar{\Upsilon}_{ij}^{\text{imu}}$, we perform uncertainty propagation on (22) by applying a first-order Taylor expansion. Taking derivatives on (22), we can incrementally update Σ_{ij}^{imu} while preintegrating applying

$$\Sigma_{i(j+1)}^{\text{imu}} = A_j^{\text{imu}} \Sigma_{ij}^{\text{imu}} A_j^{\text{imu}T} + B_j^{\text{imu}} G_j^{\text{imu}} \begin{bmatrix} Q^{\text{acc}} & 0_3 \\ 0_3 & Q^{\text{gyr}} \end{bmatrix} G_j^{\text{imu}T} B_j^{\text{imu}T} \quad (23)$$

starting from the initial condition $\Sigma_{ii}^{\text{imu}} = 0_{9 \times 9}$ where

$$A_j^{\text{imu}} = \frac{\partial \bar{\Upsilon}_{i(j+1)}}{\partial \bar{\Upsilon}_{ij}} = \frac{\partial \Phi(T)}{\partial \Phi(T)} \cdot \bar{\Upsilon}_j \frac{\partial \Phi(T, \tau)}{\partial T}$$

$$= \text{Ad} \left(\bar{\Upsilon}_j^{\text{imu}^{-1}} \right) \cdot F_{SE_2(3)}(\tau),$$

$$B_j^{\text{imu}} = \frac{\partial \bar{\Upsilon}_{i(j+1)}}{\partial \bar{\Upsilon}_j} = \frac{\partial \Phi(T)}{\partial \bar{\Upsilon}_j} \cdot \bar{\Upsilon}_j = I_9.$$

Proposition 1 provides $F_{SE_2(3)}(\tau)$ and Q models sensors noise defined in (2).

For this configuration, if a null measurement is received, the robot is in free fall, as in (20) the CGAM is considered. Therefore, a position and a velocity compensation are needed to the Γ element of the model in (12). Moreover, a rotation compensation can also be possible. Thus, at the $SE_2(3)$ group the compensation factor has the following form:

$$\Gamma^{\text{imu}} = \left[\begin{array}{c|c|c} \Gamma_R & \Gamma_p & \Gamma_v \\ \hline 0_{2 \times 3} & I_2 & \end{array} \right] \quad (24)$$

where $\Gamma_R, \Gamma_p,$ and Γ_v will be defined later in Section VI for the FEM and the REM.

C. Joint IMU and Linear Velocity Sensor Preintegration

To improve the accuracy of an INS when faults appear on the exteroceptive sensor, we propose to combine the IMU with an LVS. In this case, two independent sensors are used to form a unique pseudomeasurement, since to integrate the LVS measurements, the gyroscope information from the IMU is also needed. Thus, we propose to fuse both sensors in a unique preintegrated factor to keep all the correlation between the preintegrated IMU and the preintegrated LVS. The joint preintegration of linear accelerations, angular rates, and linear velocities is performed at the $SE_3(3)$ group

$$SE_3(3) := \left\{ T = \left[\begin{array}{c|c|c} R & p^{\text{imu}} & v & p^{\text{lvs}} \\ \hline 0_3 & I_3 & \end{array} \right] \in \mathbb{R}^{6 \times 6} \mid \begin{array}{l} R \in SO(3) \\ p^{\text{imu}}, v, p^{\text{lvs}} \in \mathbb{R}^3 \end{array} \right\}$$

where $R, p,$ and $v,$ respectively, model the robot orientation, position, and linear velocity and the group tangent space is $\varepsilon = [\phi^T, \rho^{\text{imu}T}, \nu^T, \rho^{\text{lvs}T}]^T \in \mathbb{R}^{12}$. Note that at this group the robot position is dual: p^{imu} is related to the accelerometers double integration, whereas p^{lvs} is related to the LVS integration. For a preintegrated measurement, clearly p^{imu} and p^{lvs} are different quantities as they are obtained considering different kinematic models and using different measurements. However, for any robot state, p^{imu} and p^{lvs} must be equivalent as the robot position is physically unique. Therefore, for this sensor configuration $\Upsilon \in SE_3(3)$, whereas the robot states are defined at the $SE_2(3)$ group. Keeping this in mind, to maintain the model in (12), the function $\mu : SE_2(3) \rightarrow SE_3(3)$ defined by Proposition 3 provided in the Appendix is needed to map elements from the robot state space to the measurement space where the model is declared, obtaining

$$S_j = \Gamma_{ij} \Phi_{SE_3(3)}(\mu(T_i), \Delta t) \Upsilon_{ij} \quad (25)$$

where S_j only matches $\mu(T_j)$ if there is no noise in the system and the model is exactly correct.

Considering the CGAM for the IMU measurements and a constant velocity model for the LVS measurements and considering that the IMU and the LVS may be at different frames, sensor readings are retracted to the $SE_3(3)$ group as

$$\Upsilon_k^{\text{comb}} = \left[\begin{array}{c|c|c|c} \exp(\omega_k \tau) & \frac{\tau^2}{2} a_k & \tau a_k & \tau ({}^B R_{LVS} v_k + [{}^B t_{LVS}] \times \omega_k) \\ \hline 0_3 & & & I_3 \end{array} \right] \quad (26)$$

where a_k , ω_k , and v_k follow the observation model of (2). Following a similar development as in (16), Υ_k^{comb} can be factorized into two factors

$$\Upsilon_k^{\text{comb}} \approx \bar{\Upsilon}_k^{\text{comb}} \cdot \text{Exp} \left(G_k^{\text{comb}} \begin{bmatrix} \eta^{\text{acc}} \\ \eta^{\text{gyr}} \\ \eta^{\text{lvs}} \end{bmatrix} \right) \quad (27)$$

where

$$\bar{\Upsilon}_k^{\text{comb}} = \left[\begin{array}{c|c|c|c} \exp(\hat{\omega}_k \tau) & \frac{\tau^2}{2} \hat{a}_k & \tau \hat{a}_k & \tau ({}^B R_{\text{LVS}} \hat{v}_k + [{}^B t_{\text{LVS}}]_{\times} \hat{\omega}_k) \\ \hline 0_3 & & & I_3 \end{array} \right],$$

$$G_k^{\text{comb}} = \left[\begin{array}{ccc|ccc} 0_3 & \tau J_r(\hat{\omega}_k \tau) & 0_3 & & & \\ \frac{\tau^2}{2} \exp(\hat{\omega}_k \tau)^T & 0_3 & 0_3 & & & \\ \tau \exp(\hat{\omega}_k \tau)^T & 0_3 & 0_3 & & & \\ \hline 0_3 & \tau \exp(\hat{\omega}_k \tau)^T [{}^B t_{\text{LVS}}]_{\times} & \tau \exp(\hat{\omega}_k \tau)^T B R_{\text{LVS}} & & & \end{array} \right],$$

being $\bar{\Upsilon}_k^{\text{comb}}$ a noise agnostic factor, $\hat{a}_k = \bar{a}_k - b^{\text{acc}}$, $\hat{\omega}_k = \bar{\omega}_k - b^{\text{gyr}}$ and $\hat{v}_k = \bar{v}_k - b^{\text{lvs}}$.

To incrementally compute the preintegrated measurement $\bar{\Upsilon}_{ij}^{\text{comb}}$, we apply (13). Using the definition of $\Phi_{\text{SE}_3(3)}(T, \tau)$ given by Proposition 2 provided in the Appendix and applying Lemma 1, (13) results in

$$\bar{\Upsilon}_{i(j+1)}^{\text{comb}} = \Phi_{\text{SE}_3(3)}(\bar{\Upsilon}_{ij}^{\text{comb}}, \tau) \cdot \bar{\Upsilon}_j^{\text{comb}} \quad (28)$$

which again is an incremental series. To compute the covariance matrix $\Sigma_{ij}^{\text{comb}}$ related to the preintegrated measurement $\bar{\Upsilon}_{ij}^{\text{comb}}$, we perform uncertainty propagation on (28) by applying a first-order Taylor expansion. Taking derivatives on (28), we can update $\Sigma_{ij}^{\text{comb}}$ applying

$$\begin{aligned} \Sigma_{i(j+1)}^{\text{comb}} &= A_j^{\text{comb}} \Sigma_{ij}^{\text{comb}} A_j^{\text{comb}T} \\ &+ B_j^{\text{comb}} G_j^{\text{comb}} \begin{bmatrix} Q^{\text{acc}} & 0_3 & 0_3 \\ 0_3 & Q^{\text{gyr}} & 0_3 \\ 0_3 & 0_3 & Q^{\text{lvs}} \end{bmatrix} G_j^{\text{comb}T} B_j^{\text{comb}T} \end{aligned} \quad (29)$$

starting from the initial condition $\Sigma_{ii}^{\text{comb}} = 0_{12 \times 12}$ where

$$\begin{aligned} A_j^{\text{comb}} &= \frac{\partial \bar{\Upsilon}_{i(j+1)}}{\partial \bar{\Upsilon}_{ij}} = \frac{\partial \Phi(T) \cdot \bar{\Upsilon}_j}{\partial \Phi(T)} \frac{\partial \Phi(T, \tau)}{\partial T} \\ &= \text{Ad} \left(\bar{\Upsilon}_j^{\text{comb}^{-1}} \right) \cdot F_{\text{SE}_3(3)}(\tau), \\ B_j^{\text{comb}} &= \frac{\partial \bar{\Upsilon}_{i(j+1)}}{\partial \bar{\Upsilon}_j} = \frac{\partial \Phi(T) \cdot \bar{\Upsilon}_j}{\partial \bar{\Upsilon}_j} = I_{12}. \end{aligned}$$

Proposition 2 provides $F_{\text{SE}_3(3)}(\tau)$ and Q models sensors noise defined in (2).

For this configuration, if a null measurement is received, the robot is at the same time in free fall for the IMU integrated position and remains static for the LVS integrated position, since in (26) the CGAM is considered to preintegrate the IMU measurements, whereas a constant velocity model is considered for the LVS measurements. Therefore, a position and a velocity compensation are needed at the IMU components of the Γ element in (12) to maintain the equivalence with the LVS positional part. Moreover, as for the other sensor configurations, a rotational compensation can also be considered. Thus, at the $\text{SE}_3(3)$ group the compensation factor has the following form:

$$\Gamma^{\text{comb}} = \left[\begin{array}{c|c|c} \Gamma_R & \Gamma_p & \Gamma_v \\ \hline 0_3 & & I_3 \end{array} \middle| \begin{array}{c} 0_{3 \times 1} \\ I_3 \end{array} \right] \quad (30)$$

where Γ_R , Γ_p , and Γ_v will be defined later in Section VI for the FEM and the REM.

Finally, for this configuration, we are fusing two sensors of different nature that may run at different rates. To synchronize them, we run the preintegration at the IMU rate and we consider constant linear velocity between the LVS measurements. Thus, our approach feeds the graph with two preintegration hypotheses (a constant velocity model and a constant acceleration model) making the solver responsible for deciding which option best matches the exteroceptive measurements based on uncertainty metrics.

D. Preintegration Considering Sensors Bias Estimation

A fact that we have not considered yet, is the sensors bias evolution during preintegration. Biases are unobserved variables that also have to be estimated by the Graph SLAM problem. To do it, we assume constant biases for a whole preintegrated measurement [2], [3]. However, to compute the uncertainty related to the bias evolution, we perform covariance propagation on (3) by applying a first-order Taylor expansion. Taking derivatives on (3), we can incrementally update $\Sigma_{ij}^{\text{bias}}$ while preintegrating applying

$$\Sigma_{i(j+1)}^{\text{bias}} = A_j^{\text{bias}} \Sigma_{ij}^{\text{bias}} A_j^{\text{bias}T} + B_j^{\text{bias}} Q^b B_j^{\text{bias}T} \quad (31)$$

starting from a zero initial condition where Q^b models the biases' random walk defined in (3), $A_j^{\text{bias}} = I$ and $B_j^{\text{bias}} = I$.

When the sensors bias are considered at the estimation problem, a new manifold needs to be defined to extend the problem state. We propose to use the composite manifold $\langle \text{SE}_N(3), \mathbb{R}^3, \dots, \mathbb{R}^3 \rangle$, where $\text{SE}_N(3)$ models the robot state and \mathbb{R}^3 models an euclidean base with M bias directions. For instance, for the IMU-LVS configuration (where $N = 3$ and $M = 3$) the composite manifold tangent space is

$$\varepsilon = \left[\phi^T \quad \rho^{\text{imu}T} \quad \nu^T \quad \rho^{\text{lvs}T} \quad b^{\text{acc}T} \quad b^{\text{gyr}T} \quad b^{\text{lvs}T} \right]^T \in \mathbb{R}^{21}.$$

By using a composite manifold, the group operators are obtained by the concatenation of the blocks for each component [16]. Therefore, the Jacobians for covariance propagation during preintegration can be computed per blocks

applying

$$\begin{aligned} \Sigma_{i(j+1)}^{\text{full}} &= A_j^{\text{full}} \Sigma_{ij} A_j^{\text{full}T} \\ &+ B_j^{\text{full}} \begin{bmatrix} Q^n & 0_{(3N+3) \times 3M} \\ 0_{3M \times (3N+3)} & Q^b \end{bmatrix} B_j^{\text{full}T} \end{aligned} \quad (32)$$

starting from the initial condition $\Sigma_{ii} = 0_{(3N+3+3M) \times (3N+3+3M)}$ where

$$\begin{aligned} A_j^{\text{full}} &= \left[\begin{array}{c|c} A_j^{\text{sensor}} & -G_j^{\text{sensor}} \\ \hline 0_{3M \times 3N+3} & A_j^{\text{bias}} \end{array} \right] \in \mathbb{R}^{(3N+3+3M) \times (3N+3+3M)}, \\ B_j^{\text{full}} &= \left[\begin{array}{c|c} G_j^{\text{sensor}} & 0_{(3N+3) \times 3M} \\ \hline 0_{3M \times 3M} & B_j^{\text{bias}} \end{array} \right] \in \mathbb{R}^{(3N+3+3M) \times 6M}, \end{aligned}$$

and sensor noise Q^n and bias random walk Q^b are, respectively, defined in (2) and (3). $A_j^{\text{sensor}} \in \mathbb{R}^{(3N+3) \times (3N+3)}$ and $G_j^{\text{sensor}} \in \mathbb{R}^{(3N+3) \times 3M}$ are defined in (18), (23), or (29) depending on the applied sensor configuration and $A_j^{\text{bias}}, B_j^{\text{bias}} \in \mathbb{R}^{3M \times 3M}$ are defined in (31). Note that the preintegrated measurements depend on the sensor biases. Following the observation model defined in (2), bias and noise are small additive quantities to the measurements. Thus, the derivative of the preintegrated model through the sensor biases is the same as the derivative through the sensor noise.

VI. PREINTEGRATION RESIDUALS

After aggregating sensor measurements into preintegrated measurements, residuals for these quantities can be evaluated. Preintegrated measurements have been computed assuming a predefined constant sensor biases. However, sensor biases are estimated variables whose estimation is improved while solving the problem. Thus, preintegration measurements must be updated accordingly. In the following, first, we review a mechanism to update preintegrated measurements when the biases change, avoiding rebuilding the preintegration. Then, we introduce the preintegrated residuals at the $SE_N(3)$ group for the FEM and the REM, paying special attention to the mathematical calculation of the Jacobians and providing its analytical form.

A. Bias Correction

To avoid reintegrating from scratch all the measurements that form a preintegrated measurement when the estimation for its associated bias is refined, the measurement can be updated by performing a first-order Taylor expansion of (13) on the biases [2] considering the $SE_N(3)$ group. Thus, a preintegrated measurement is built by assuming constant bias \hat{b}_i , for instance, the bias estimation for the previous key frame. Then, when new estimations b_i are available, the preintegrated measurement can

be updated applying

$$\bar{\Upsilon}_{ij}(b_i) = \bar{\Upsilon}_{ij}(\hat{b}_i) \oplus J_{ij}(b_i - \hat{b}_i) \quad (33)$$

where $\bar{\Upsilon}_{ij}(\hat{b}_i)$ is the preintegrated measurement assuming \hat{b}_i and $J_{ij} = \frac{\partial \bar{\Upsilon}_{ij}}{\partial b_i} \Big|_{\hat{b}_i}$ is the derivative of the preintegrated measurement through the bias evaluated at the bias assumption \hat{b}_i . Following [24], this derivative can be incrementally computed while preintegrating by applying

$$J_{i(j+1)} = A_j J_{ij} - G_j \quad (34)$$

where A_j and G_j are defined in (18), (23), or (29), depending on the chosen sensor configuration.

B. FEM Residual

The FEM is a preintegration approximation that only considers gravity as an external perturbation. The continuous-time analytical model for this approach is

$$\begin{aligned} {}^W \dot{R}_B &= {}^W R_B [{}^B \omega]_{\times}, \\ {}^W \dot{v} &= {}^W R_B {}^B a + g, \\ {}^W \dot{p}_B &= {}^W v, \end{aligned} \quad (35)$$

where ${}^W R_B$, ${}^W v$, and ${}^W p_B$ are, respectively, the orientation, linear velocity, and position of the robot at the world frame. Considering the preintegration model given in (12), the compensation components for the FEM are [3]

$$\Gamma_R = I_3, \quad \Gamma_p = \frac{\Delta t^2}{2} g, \quad \Gamma_v = \Delta t g, \quad (36)$$

where Δt is the elapsed time during the preintegration of $\bar{\Upsilon}_{ij}$.

Given a preintegrated measurement $\bar{\Upsilon}_{ij}$ and its associated covariance matrix Σ_{ij} , considering the residual definition in (14), the bias update in (33), and the mapping $\mu(T)$ applied in (25); the residual between robot states T_i and T_j is

$$\begin{aligned} r_{ij} &= \\ &\Sigma_{ij}^{-1/2} \text{Log} \left\{ \bar{\Upsilon}_{ij}^{-1} \cdot \Phi(\mu(T_i), \Delta t)^{-1} \cdot \Gamma_{ij}^{-1} \cdot \mu(T_j) \cdot \text{Exp}(-J_{ij} \delta b_i) \right\} \end{aligned} \quad (37)$$

where $\delta b_i = (b_i - \hat{b}_i)$, J_{ij} is provided by (34) and the definitions for $\Phi(T, \Delta t)$ and $\mu(T)$ are listed in Table II. The derivatives of the residual through the robot poses T_i and T_j and the sensor bias b_i at the $SE_N(3)$ group are

$$\begin{aligned} \frac{\partial r}{\partial T_i} &= \frac{\partial \text{Log}(L)}{\partial L} \frac{\partial \bar{\Upsilon}_{ij}^{-1}}{\partial K} \cdot K \frac{\partial \Phi^{-1} \cdot Y}{\partial \Phi^{-1}} \frac{\partial \Phi^{-1}}{\partial \Phi} \frac{\partial \Phi(\mu(T_i), \Delta t)}{\partial \mu(T_i)} \frac{\partial \mu(T_i)}{\partial T_i} \\ &= -J_r(L)^{-1} \text{Ad}(Y^{-1} \cdot \Phi(\mu(T_i), \Delta t)) F(\Delta t) M, \\ \frac{\partial r}{\partial T_j} &= \frac{\partial \text{Log}(L)}{\partial L} \frac{\partial R \cdot S}{\partial S} \frac{\partial \mu(T_j)}{\partial \mu(T_j)} \cdot \text{Exp}(\lambda) \frac{\partial \mu(T_j)}{\partial T_j} \\ &= J_r(L)^{-1} \text{Ad}(\text{Exp}(J_{ij} \delta b_i)) M, \\ \frac{\partial r}{\partial b_i} &= \frac{\partial \text{Log}(L)}{\partial L} \frac{\partial C \cdot \text{Exp}(\lambda)}{\partial \text{Exp}(\lambda)} \frac{\partial \text{Exp}(\lambda)}{\partial \lambda} \frac{\partial \lambda}{\partial b_i} \\ &= -J_r(L)^{-1} J_r(-J_{ij} \delta b_i) J_{ij}, \end{aligned} \quad (38)$$

TABLE II
LIE GROUPS AND FUNCTIONS NEEDED FOR THE ANALYZED SENSORS CONFIGURATIONS

Sensors configuration	N	M	Robot state	Measurement	Preintegration map	State map	REM map
Gyros + LVS	1	2	$X \in \text{SE}(3)$	$\Upsilon \in \text{SE}(3)$	$\Phi_{\text{SE}(3)}(T, \Delta t) = T$	$\mu_{\text{SE}(3)}(T) = T$	$\psi_{\text{SE}(3)}(T) = T$
IMU	2	2	$X \in \text{SE}_2(3)$	$\Upsilon \in \text{SE}_2(3)$	Proposition 1	$\mu_{\text{SE}_2(3)}(T) = T$	Proposition 4
IMU + LVS	3	3	$X \in \text{SE}_2(3)$	$\Upsilon \in \text{SE}_3(3)$	Proposition 2	Proposition 3	Proposition 5

Propositions are provided in the Appendix.

where

$$L = \underbrace{\bar{\Upsilon}_{ij}^{-1} \cdot \Phi(\mu(T_i), \Delta t)^{-1} \cdot \Gamma_{ij}^{-1}}_R \cdot \underbrace{\mu(T_j) \cdot \text{Exp}(-J_{ij} \delta b_i)}_S$$

$$= \underbrace{\bar{\Upsilon}_{ij}^{-1} \cdot \Phi(\mu(T_i), \Delta t)^{-1} \cdot \Gamma_{ij}^{-1} \cdot \mu(T_j)}_K \cdot \text{Exp}(-J_{ij} \delta b_i),$$

$$\lambda = -J_{ij} \delta b_i.$$

$\text{Exp}(T)$, $\text{Log}(T)$, $\text{Ad}(T)$, and $\text{Jr}(T)$ are defined in Section IV-A and $F(\Delta t) = \frac{\partial \Phi(T, \Delta t)}{\partial T}$ and $M = \frac{\partial \mu(T)}{\partial T}$ are provided by the Propositions listed in Table II.

C. REM Residual

The REM is a preintegration approximation that considers gravity and Earth rotation as external perturbations. The analytical model for this approach is

$$\begin{aligned} {}^W \dot{R}_B &= {}^W R_B [{}^B \omega]_{\times} - [\Omega]_{\times} {}^W R_B, \\ {}^W \dot{v} &= {}^W R_B {}^B a + g - 2[\Omega]_{\times} {}^W v - [\Omega]_{\times}^2 {}^W p_B, \\ {}^W \dot{p}_B &= {}^W v, \end{aligned} \quad (39)$$

where Ω is the Earth rotation rate vector defined in (1). To express this model in the form of the preintegration model in (12), an automorphism $\psi : \text{SE}_N(3) \rightarrow \text{SE}_N(3)$ applied to the robot state is needed [24]. By applying the definitions of $\psi(T)$ listed in Table II, the continuous model becomes

$$N_j = \Gamma_{ij} \Phi(\psi(T_i), \Delta t) \Upsilon_{ij}, \quad (40)$$

where Δt is the elapsed time during the preintegration of $\bar{\Upsilon}_{ij}$ and N_j only matches $\psi(T_j)$ if there is no noise in the system and the model is exactly correct. The compensation components for this model are [24]

$$\begin{aligned} \Gamma_R &= \exp(\Delta t \Omega)^T, \\ \Gamma_p &= \left(\frac{\Delta t^2}{2} I_3 + a[\Omega]_{\times} + b[\Omega]_{\times} \right) g, \\ \Gamma_v &= J_r(-\Delta t \Omega) \Delta t g, \end{aligned} \quad (41)$$

where $\theta = \|\Omega\|$ and

$$\begin{aligned} a &= \frac{1}{\theta^3} \left(\Delta t \theta \cos(\Delta t \theta) - \sin(\Delta t \theta) \right), \\ b &= \frac{1}{\theta^4} \left(\frac{\Delta t^2 \theta^2}{2} - \cos(\Delta t \theta) - \Delta t \theta \sin(\Delta t \theta) + 1 \right). \end{aligned}$$

Given a preintegrated measurement $\bar{\Upsilon}_{ij}$ and its associated covariance matrix Σ_{ij} , considering the residual definition in (14), the bias update in (33), and the functions $\mu(T)$ and $\psi(T)$, respectively, applied in (25) and (40); the residual between robot states T_i and T_j is

$$r_{ij} = \Sigma_{ij}^{-1/2} \text{Log} \left\{ \bar{\Upsilon}_{ij}^{-1} \cdot \Phi(\psi(\mu(T_i)), \Delta t)^{-1} \cdot \Gamma_{ij}^{-1} \cdot \psi(\mu(T_j)) \cdot \text{Exp}(-J_{ij} \delta b_i) \right\} \quad (42)$$

where $\delta b_i = (b_i - \hat{b}_i)$, J_{ij} is provided by (34) and the definitions for $\Phi(T, \Delta t)$, $\psi(T)$, and $\mu(T)$ are listed in Table II. The derivatives of the residual through the robot poses T_i and T_j and the sensors bias b_i at the Special Euclidean N group $\text{SE}_N(3)$ ($\text{SE}_N(3)$) group are as follows:

$$\begin{aligned} \frac{\partial r}{\partial T_i} &= \frac{\partial \text{Log}(L)}{\partial L} \frac{\partial \bar{\Upsilon}_{ij}^{-1} \cdot K}{\partial K} \frac{\partial \Phi^{-1} \cdot Y}{\partial \Phi^{-1}} \frac{\partial \Phi^{-1}}{\partial \Phi} \frac{\partial \Phi(\psi, \Delta t)}{\partial \psi} \frac{\partial \psi(\mu)}{\partial \mu} \frac{\partial \mu(T_i)}{\partial T_i} \\ &= -J_r(L)^{-1} \text{Ad}(Y^{-1} \cdot \Phi(\psi(\mu(T_i)), \Delta t)) F(\Delta t) \Psi(\mu(T_i)) M, \\ \frac{\partial r}{\partial T_j} &= \frac{\partial \text{Log}(L)}{\partial L} \frac{\partial R \cdot S}{\partial S} \frac{\partial \psi \cdot \text{Exp}(\lambda)}{\partial \psi} \frac{\partial \psi(\mu)}{\partial \mu} \frac{\partial \mu(T_j)}{\partial T_j} \\ &= J_r(L)^{-1} \text{Ad}(\text{Exp}(J_{ij} \delta b_i)) \Psi(\mu(T_j)) M, \\ \frac{\partial r}{\partial b_i} &= \frac{\partial \text{Log}(L)}{\partial L} \frac{\partial C \cdot \text{Exp}(\lambda)}{\partial \text{Exp}(\lambda)} \frac{\partial \text{Exp}(\lambda)}{\partial \lambda} \frac{\partial \lambda}{\partial b_i} \\ &= -J_r(L)^{-1} J_r(-J_{ij} \delta b_i) J_{ij}, \end{aligned} \quad (43)$$

where

$$L = \underbrace{\bar{\Upsilon}_{ij}^{-1} \cdot \Phi(\psi(\mu(T_i)), \Delta t)^{-1} \cdot \Gamma_{ij}^{-1}}_R \cdot \underbrace{\psi(\mu(T_j)) \cdot \text{Exp}(-J_{ij} \delta b_i)}_S$$

$$= \underbrace{\bar{\Upsilon}_{ij}^{-1} \cdot \Phi(\psi(\mu(T_i)), \Delta t)^{-1} \cdot \Gamma_{ij}^{-1} \cdot \psi(\mu(T_j))}_K \cdot \text{Exp}(-J_{ij} \delta b_i),$$

$$\lambda = -J_{ij} \delta b_i.$$

$\text{Exp}(T)$, $\text{Log}(T)$, $\text{Ad}(T)$, and $Jr(T)$ are defined in Section IV-A and $F(\Delta t) = \frac{\partial \Phi(T, \Delta t)}{\partial T}$, $\Psi(T) = \frac{\psi(T)}{\partial T}$, and $M = \frac{\partial \mu(T)}{\partial T}$ are provided by the Propositions listed in Table II.

VII. EXPERIMENTAL SETUP

In this experiment, we test the proposed preintegration methodology on an AUV that uses a DVL as the LVS. In the following sections, we describe the navigation algorithm and the robotic platform used to validate the proposed tool in real experiments performed at open sea.

A. Underwater Dead Reckoning Algorithm

Combining the preintegrated factor with the factors introduced in a previous work [36], the chained factor graph of Fig. 1 is built. This graph models a dead reckoning problem, defining a graph-based INS. Compared to a filter-based solution, this proposal allows perception constraints to be easily added to the problem by closing loops on the chained graph, converting the dead reckoning approach into a Graph SLAM problem. Algorithm 1 establishes the navigation methodology. In this problem, key frames are set at a constant rate, whereas in a Graph SLAM problem, key frames are set when a new relevant measurement from the robot surroundings is received. In the underwater domain, exteroceptive measurements can be, for example, an acoustic signal received from a beacon or a point cloud gathered by a sonar scanner.

Following Algorithm 1, first, the sensors are initialized, the North East Down (NED) reference frame is established and a guess for the robot initial pose is estimated using a GNSS. By considering a graph approach, an imprecise initial condition is sufficient as the initial orientation of the robot will be improved as the problem grows, thanks to the global actions measured by the IMU: the gravity and the Earth rotation. Once the initial condition is set, the estimation problem starts and GNSS measurements are no longer considered by this navigator.

Between the reception of key frames, the IMU and DVL preintegration is running. When a new key frame is received, the preintegration is stopped, the result is stored and a new preintegrated measurement is started. Using the obtained preintegrated measurement, a preintegrated factor is set between the current key frame and the previous one. Moreover, the linear velocity and pressure priors are set to the current key frame using the newest DVL and pressure measurements [36]. Finally, combining the estimation for the previous key frame with the preintegrated measurement, a seed for the current key frame is provided to the solver. By using the $iSAM2$ solver [37], which is an incremental solver, the problem is solved every time a new key frame is set, giving an online AUV navigator estimating the whole robot trajectory.

B. Robot Setup

Sea experiments have been carried using the Girona 1000 AUV [38] – from IQUA Robotics, Girona (Catalonia) – a reconfigurable underwater platform suitable for intervention and surveying that is equipped with several proprioceptive sensors.

Algorithm 1: Graph-Based Inertial Navigation System.

```

Initialize IMU, DVL, SVS and GNSS
Set NED reference frame
Set gravity acceleration direction at NED
Set Earth rotation rate direction at NED
Initialize the navigation factor graph
Set pose, linear velocity and biases priors
Set initial pose, linear velocity and biases seeds
Loop
  if not key frame received then
    Preintegrate IMU and DVL measurements
  else
    Set a preintegrated factor and reset preintegration
    Set a seed for the new key frame
    Set a linear velocity prior to the new key frame1
    Set a pressure prior to the new key frame
    Solve the navigation factor graph
  end if
end loop

```

Linear accelerations and angular velocities are provided by a Phins Compact C3 INS – from iXblue, Saint-Germain en Laye (France) – a navigational grade INS based on FOG and MEMS accelerometers that is used as an IMU by reading the raw sensor measurements. Linear velocity is measured by a DVL1000–4000 m – from Nortek, Rud (Norway) – which is assembled at the lower AUV cylinder pointing the seabed. Water pressure is provided by a miniSVS1000 – from Valeport Ltd, Totnes (United Kingdom) – a Sound Velocity Sensor (SVS) measuring pressure and sound velocity. Finally, the AUV position at surface is provided by an L86 – from Quectel, Shanghai (China) – a compact GNSS mounted at the AUV antenna. All sensors are connected to the Phins Compact C3 INS to run the commercial iXblue INS algorithm, a filter-based INS applying an Unscented Kalman Filter (UKF). Fig. 4 shows the poses of the sensors on the AUV and Table III provides the values extracted from the CAD drawings.

Experiments were carried in front of the Sant Feliu de Guixols harbor (Girona, Catalonia) at shallow waters of 15–20 m depth with a flat seabed. During the experiments, the AUV was deployed at surface. Through this set up, the DVL could measure the AUV linear velocity against the seafloor and the AUV antenna was not submerged, providing GNSS measurements for the duration of the trajectory. The GNSS was disabled on the iXblue INS filter to simulate an underwater performance. Thus, GNSS measurements are used as the AUV ground truth to benchmark the proposed navigator against the iXblue INS filter in equal conditions of information. No GNSS deviation is considered, as the duration and extension of the experiments are not significant in terms of deviation.

Finally, Table IV shows the temporal rates for the sensors and the navigator. Although the rates for the SVS and the DVL are given, the DVL is preintegrated at the IMU rate and prior factors are set at the navigator rate. Therefore, these values are only provided to show that these sensors are much faster than

¹Only applied to IMU-only preintegration setups to account for LVS data.

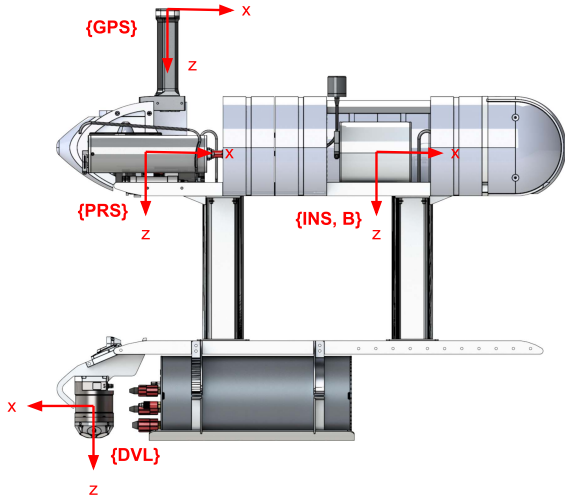


Fig. 4. Pressure sensor {PRS}, INS {INS}, DVL {DVL} and GPS {GPS} mounted on the Girona 1000 AUV {B}.

TABLE III
GIRONA 1000 AUV GEOMETRIC PARAMETERS

Sensor	Level Arm [mm]	Rotation (RPY) [°]
DVL	-898.65, -377.25, -783.55	0, 0, 180
Pressure	-825.70, -27.25, 129.45	0, 0, 0

TABLE IV
SENSOR AND SYSTEM RATES

System	Rate [Hz]
IMU	100.0
SVS	8.0
DVL	4.0
Pose graph node creation applying IMU preintegration	0.4
Pose graph node creation applying DVL preintegration	0.2

TABLE V
SENSOR NOISE AND BIAS RANDOM WALK

Description	Symbol	Standard deviation σ
Accelerometer	η^{acc}	1.0 m/(s ² √Hz)
Gyroscope	η^{gr}	1e-3 rad/(s√Hz)
Accelerometer bias random walk	η^{ba}	1e-3 m/(s ² √Hz)
Gyroscope bias random walk FEM	η^{bg}	1e-5 rad/(s√Hz)
Gyroscope bias random walk REM	η^{bg}	1e-6 rad/(s√Hz)
Pressure	η^{ps}	0.5 m
DVL	η^{dvl}	1e-1 m/(s√Hz)
DVL bias random walk	η^{bd}	1e-3 m/(s√Hz)
AUV position prior	η^{p0}	0.5 m
AUV orientation prior	η^{phi0}	1e-2 rad
AUV linear velocity prior	η^{v0}	1e-1 m/s
Accelerometer bias prior	η^{ba0}	1e-3 m/s ²
Gyroscope bias prior	η^{bg0}	1e-3 rad/s
DVL bias prior	η^{bd0}	1e-3 rad/s

the navigator and, using the closest measurement to each key frame, are a good approximation to set the prior factors. Table V shows the noise and bias random walk standard deviation considered for the sensors, tuned according to the sensor data sheet. The only remarkable fact is that gyroscope bias random walk must change when considering the FEM or the REM, as

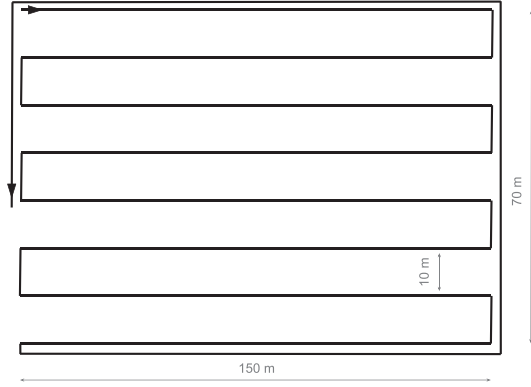


Fig. 5. Survey followed by Girona 1000 AUV.

will be discussed according to the results. Finally, the noise for the priors set to the initial condition is provided.

VIII. RESULTS

The navigator is tested on a surface survey for 1 h, covering an area of 150 × 70 m in corridors of 10 m width. At the end of the survey, the AUV turned around the perimeter of the surveyed area (see Fig. 5). The AUV moved along the surface at an average forward velocity of 0.5 m/s. Many experiments were done, doing several iterations and obtaining systematic results. Thus, all the presented tests were done using the same dataset to ease the comparison.

A. IMU-Only Preintegration Considering the FEM

In this experiment, we used a navigator that performs IMU-only preintegration considering the FEM. This setup applies the state-of-the-art preintegration methodology [3] since the DVL is not preintegrated, missing lots of measurements as only a small portion is used to set velocity priors, and no Earth rotation compensation is considered, although using a navigational grade IMU sensitive to the Earth rotation.

Fig. 6(a) shows the top view of the trajectory followed by the AUV. GNSS measurements, in blue, are considered as the robot ground truth. The estimation provided by the iXblue INS filter is plotted in red and the smoothed trajectory estimated by the proposed navigator is plotted in purple. Fig. 6(b) plots the positional error accumulated through the robot trajectory by the iXblue INS filter and by our proposal, both calculated against the GNSS measurements. The error is given in NED components and its euclidean norm is also provided. The same color code of Fig. 6(a) is maintained. Finally, Fig. 7(a) shows the estimated IMU biases. In red, we have plotted the estimation for the last key frame set at each solver call, whereas in blue, we have plotted the whole smoothed bias trajectory obtained at each solver call.

B. IMU-Only Preintegration Considering the REM

In this experiment, we applied the same setup as in the previous experiment, only substituting the FEM with the REM to compensate the Earth rotation rate measured by the IMU. This navigator was inspired by the methodology proposed at [24].

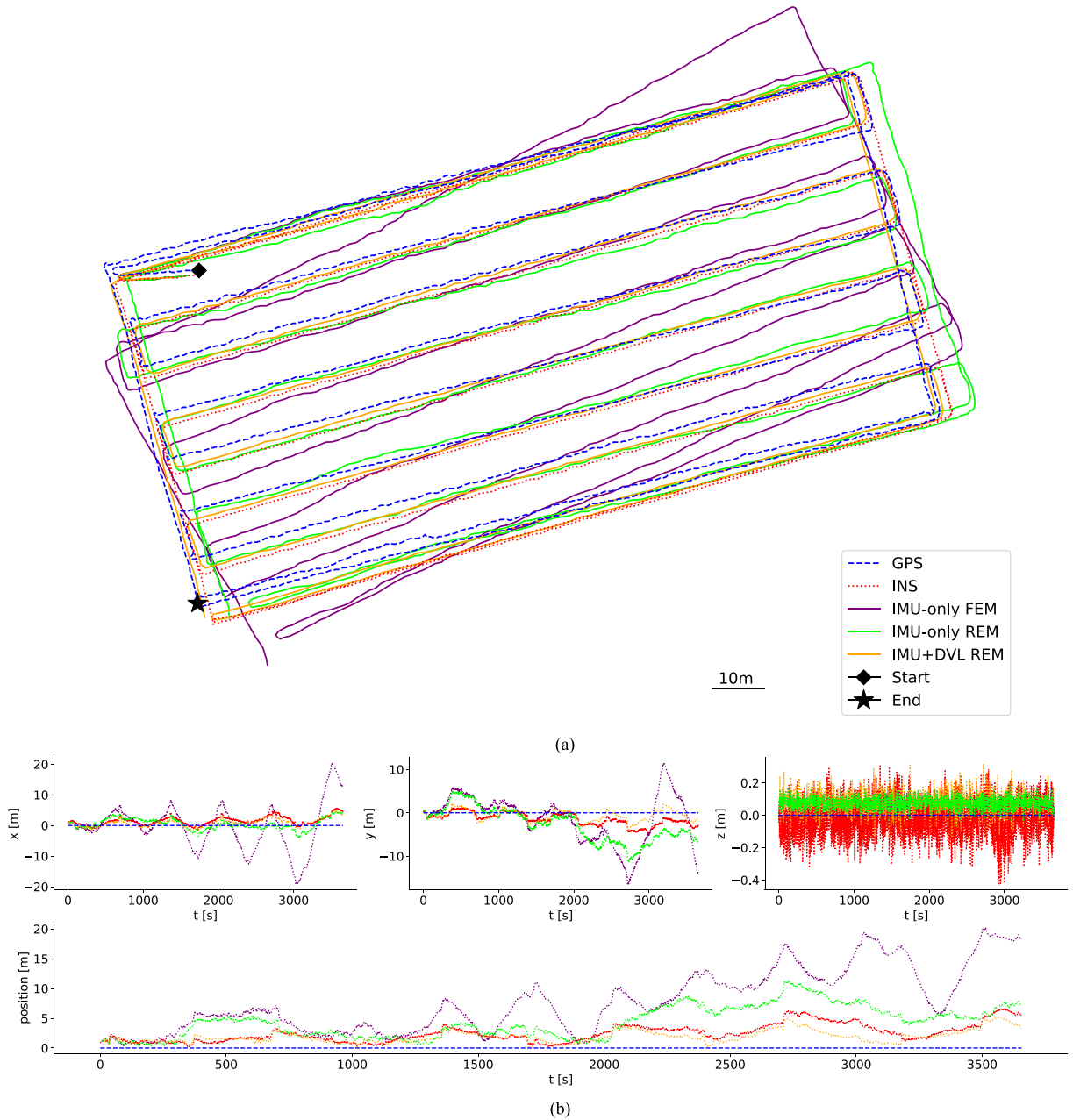


Fig. 6. Estimated trajectory for the proposed navigators compared to GNSS measurements and the iXblue INS filter estimation. (a) AUV trajectory on an x and y projection at the world frame. (b) Positional error time evolution. Top: x , y , and z components (left to right). Bottom: Euclidean norm.

Fig. 6(a) shows, in green, the top view of the estimated trajectory of the AUV, whereas Fig. 6(b) plots the accumulated positional error. Finally, Fig. 7(b) shows the estimated bias for the IMU.

C. Joint IMU and DVL Preintegration Considering the REM

In this experiment, we applied a navigator combining the joint IMU and DVL preintegration with the REM. This setup corresponds to our contribution, as an IMU sensitive to the Earth rotation is compensated and all DVL measurements are

preintegrated to mitigate the robot drift. Fig. 6(a) shows, in orange, the smoothed AUV trajectory, whereas Fig. 6(b) plots the accumulated positional error. Finally, Fig. 7(c) shows the estimated IMU and DVL biases. Note that this setup allows to estimate the DVL bias. To provide a broader experimentation of our contribution, we prove this navigator under equal conditions on other datasets, described by the duration and the AUV mean velocity. Table VI provides the error for the last robot position and the positional Root Mean Squared Error (RMSE) through the AUV trajectory between our navigator, the GNSS measurements and the iXblue INS estimation.

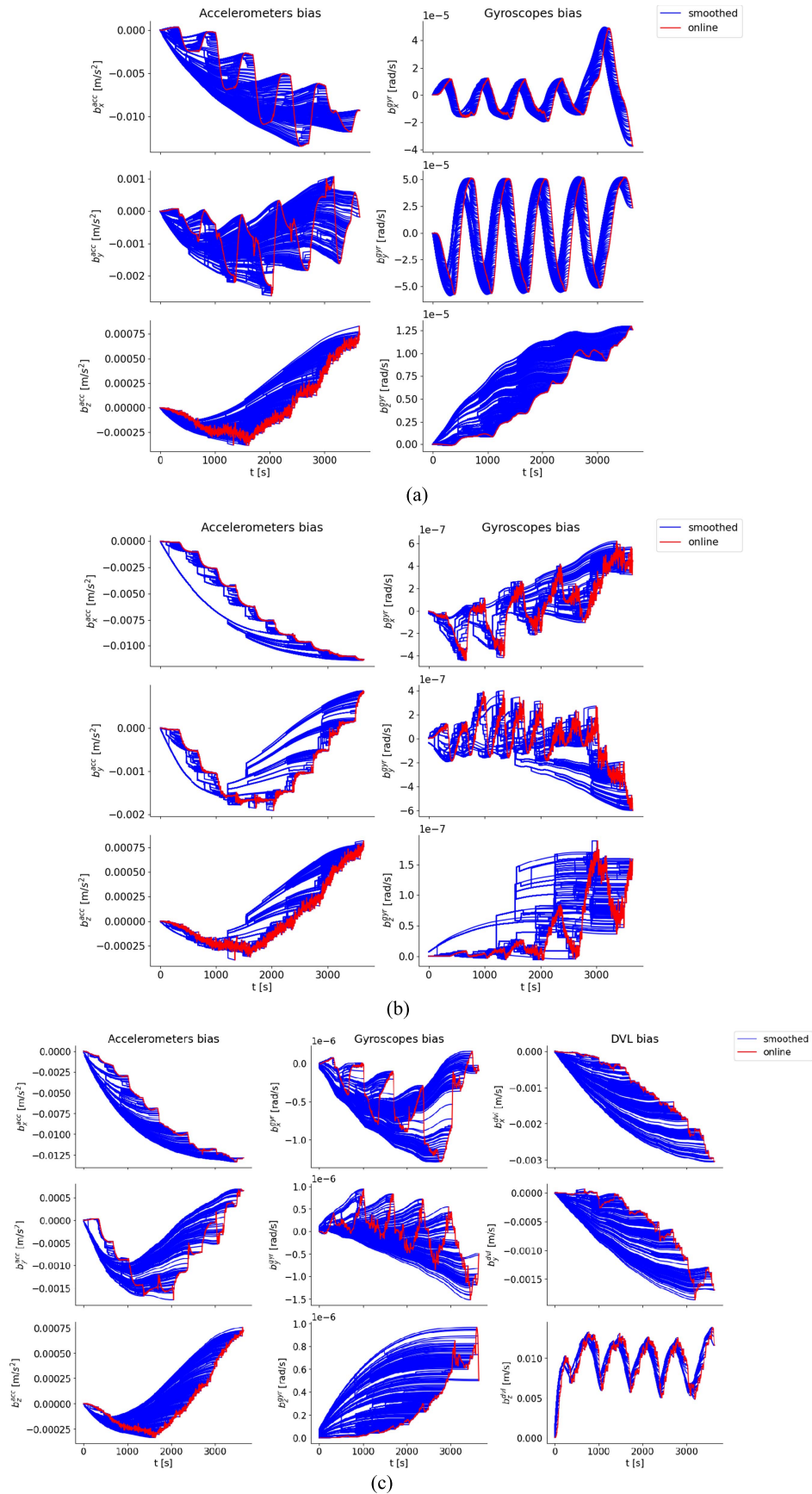


Fig. 7. Online sensor biases estimation (red) and smoothed sensor biases trajectory (blue) for all the graph key frames. (a) IMU-only preintegration considering the flat earth model. (b) IMU-only preintegration considering the rotating earth model. (c) Joint IMU and DVL preintegration considering the rotating earth model.

TABLE VI
LAST POSITION ERROR (LPE) AND POSITIONAL ROOT MEAN SQUARE ERROR (PRMSE) THROUGH THE AUV TRAJECTORY BETWEEN DIFFERENT SYSTEMS AND DATASETS UNDER EQUAL CONDITIONS

Dataset	Duration	Mean velocity	LPE our/GNSS	LPE INS/GNSS	PRMSE our/GNSS	PRMSE INS/GNSS	PRMSE our/INS
Paper	3655 s	0.48 m/s	3.288 m	5.426 m	2.090 m	2.872 m	1.384 m
Test B	3735 s	0.49 m/s	6.248 m	5.091 m	4.517 m	4.091 m	1.209 m
Test C	1405 s	0.84 m/s	14.863 m	11.307 m	6.438 m	7.006 m	3.103 m

“our” stands for our system applying the joint IMU and DVL preintegration considering the REM and “INS” is the commercial Ixblue INS estimation.

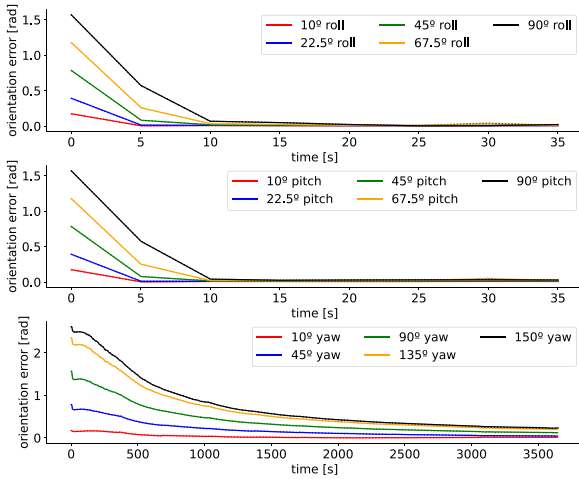


Fig. 8. Orientation error on the first robot key frame (solid) and on the current AUV pose (dotted). Dotted lines match solid lines almost perfectly and are almost not visible. Top to bottom: pure x , y , and z rotation misalignment.

D. Recovery From Bad Initialization

In this experiment, we applied the same navigator as in Section VIII-C. However, we relaxed the AUV orientation prior to 1.0 rd and we perturbed the initial AUV orientation to test how a graph-based navigator can recover from an incorrect initialization. We applied separately pure misalignments on the initial x , y and z orientations. For the roll and pitch rotations we applied misalignments up to 90° , whereas for the yaw orientation we applied misalignments up to 150° . Fig. 8 shows the orientation error evolution, computed against the iXblue INS filter estimation as no orientation ground truth can be measured in a real experiment. The continuous line plots the error for the first key frame, and the dotted line plots the error for the current robot orientation.

IX. DISCUSSION

Analyzing the results for the experiment proposed in Section VIII-A shown in Fig. 6, we see that this navigator setup does not properly estimate the robot trajectory. Drift appears on the estimation since a navigational grade IMU sensitive to the Earth rotation is used but this perturbation is not considered by the preintegration model. To resolve this, the navigator tries to compensate the perturbation in the gyroscope biases. Analysing the right plots of Fig. 7(a), at the x and y components, an oscillation appears to have the same order of magnitude as the Earth rotation rate that matches with the AUV trajectory. As the Earth rotation rate is a constant global vector and the gyroscopes are moving with the robot, every time that the AUV turns 180° to follow a new survey transect, the perceived Earth rotation rate

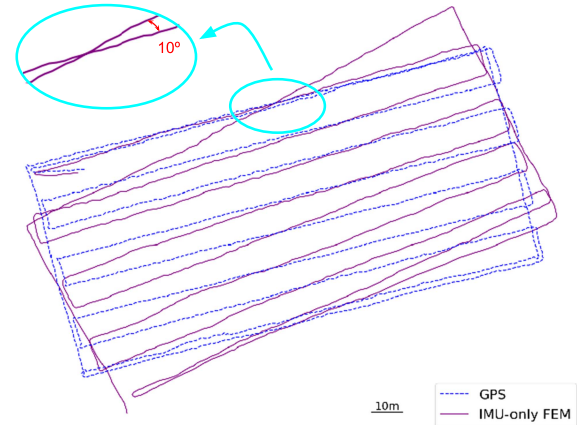


Fig. 9. Smoothed AUV trajectory obtained by the IMU-only navigator considering the FEM (purple) and GNSS measurements (blue) proving how the Earth rotation rate is integrated.

swaps direction. However, this compensation of the perturbation is not possible at the z component of the gyroscope bias, which presents a growing tendency, since the problem is not observable for the z orientation of the robot when considering the FEM. Therefore, it is impossible for the navigator to compensate for the Earth rotation perturbation in this direction, implying that a constant rotation rate is integrated, generating the twist of the trajectory shown at Fig. 6(a). In particular for this experiment, the z component of the Earth rotation rate at the NED reference is $2.78 \cdot 10^{-3}^\circ/\text{s}$. Integrating this value for the one hour survey we obtain the 10° that can be measured at Fig. 9.

The results for this experiment clearly show that the Earth rotation effect must be compensated when using a navigational grade IMU. One way of doing this is to use exteroceptive measurements by defining a SLAM problem that makes the problem observable. Otherwise, to maintain a dead reckoning approach, the estimation can be improved by considering the REM for IMU preintegration, by removing the undesired perturbation when evaluating residuals. This second option also has benefits for the bias estimation. Biases are modeled as slow time-varying quantities by imposing a Brownian motion. Having to compensate for the Earth rotation, this hypothesis on the bias dynamics fails, implying some undesired performance.

Analyzing the results for the experiment proposed in Section VIII-B we see that, by considering the REM, the navigation map and the positional error in Fig. 6 are more consistent with the position ground truth. We quantify in Fig. 6(b) that the maximum positional error for this navigator has been reduced to 12 m, not yet matching the 6 m accuracy of the iXblue INS filter. Furthermore, in Fig. 7(b), we observe that the gyroscope biases

estimation is much smaller than in the previous experiment, two orders of magnitude less than the Earth rotation rate. This behavior confirms that the REM performs well the Earth rotation compensation. Thus, the bias can model other phenomena with slower dynamics closer to that imposed by the Brownian motion. As the bias evolution is now less significant, we can reduce the dynamics of the Brownian motion as it is parameterized in Table V. Moreover, analyzing the accelerometer biases we see that, in comparison to the previous experiment, they are also free from an oscillatory behaviour. This is another benefit of considering the REM, as due to the problem correlation the Earth rotation compensation also have implications on the accelerometers bias. However, we observed no effect in enhancing the REM with Coriolis and Centrifugal contributions due to Earth rotation on the accelerometer readings.

The results for the experiment proposed in Section VIII-C show that by jointly preintegrating the IMU and the DVL, an estimation slightly better than the obtained by the iXblue INS filter is obtained. The positional error evolution plotted in Fig. 6(b) shows a similar behavior for both systems, following the same trend and magnitude for all axes. Contrary to what is expected from the literature, the graph-based navigator does not substantially outperform a filter-based solution since a dead reckoning problem is solved and linearization errors cannot be accumulated. The advantage for graph-based systems would be appreciated in a Simultaneous Localization and Mapping (SLAM) problem, where the application of exteroceptive data implies error accumulation. Compared to filter-based systems, extending the dead reckoning problem into SLAM is easy following our approach due to the graph representation of the problem.

The results for this experiment show that by jointly preintegrating IMU data with linear velocity measurements, the robustness of the navigation system increases, as it is able to increase the time elapsed between perception key frames. In comparison to the previous experiment, the navigator rate can now be halved while improving the estimation, as shown in Table IV. This feature is very interesting for managing smaller graphs while maintaining a robust odometry estimation during perception outages. Thus, DVL preintegration helps to estimate the IMU biases and reduce the drift during perception faults. Moreover, the DVL bias can also be estimated, as shown in Fig. 7(c) (right). This estimation allows compensation of incorrect measurements of the DVL level arm or of the water sound speed due to the salinity gradient through the water column. In conclusion, through this experiment we demonstrated that by preintegrating a DVL jointly with a navigational grade IMU compensated from Earth rotation, perception faults of at least 1 h can be handled correctly. Systematic results are obtained on other datasets, as it is shown in Table VI. The positional error between the systems is coherent for all datasets, and our navigator and the commercial iXblue INS show similar performance.

Finally, the experiment proposed at Section VIII-D proves how a graph-based navigator can recover from a bad initialization. By applying misalignments up to 90° in roll and pitch and 150° in yaw, the error on the estimation for the first key frame is removed following different time constants depending

on the orientation direction. For roll and pitch misalignments, the system can recover in seconds as these directions are observed by measuring the gravity that has a considerable value (9.81 m/s^2). On the contrary, for a yaw misalignment, the system needs minutes to recover as the yaw becomes observable by measuring the Earth rotation rate that has a very small value ($15^\circ/\text{h}$). Thus, to correct this misalignment, time is needed to integrate rotational error and perceive it.

X. CONCLUSION

In this article, we presented a general purpose methodology to jointly preintegrate IMU and linear velocity measurements at the $SE_N(3)$ group preserving all the existing correlation within the preintegrated quantity. Linear velocity measurements, obtained by different methodologies such as leg odometry, visual odometry or a DVL, increase the accuracy of the dead reckoning estimation and increase the stability of the navigation system to handle perception outages preventing the degeneration of the IMU bias estimation. Moreover, this methodology is suitable for higher grade IMUs sensitive to the Earth rotation, being able to consider the REM during preintegration. Finally, the proposed methodology applies a rigorous on-manifold formulation to propagate the problem uncertainty thanks to the introduction of the $SE_N(3)$ group.

Field experiments testing the proposed methodology are reported. A dead reckoning problem was solved using an AUV equipped with a DVL and a navigational grade IMU. The AUV acted as a surface vehicle to obtain GNSS measurements to evaluate different navigator setups. Results showed that by jointly preintegrating the IMU and the LVS and considering the Earth rotation compensation, we can obtain an estimation that slightly outperforms the output of a commercial filter-based INS, proving the capabilities of our graph-based system. Furthermore, our proposal can easily be extended to a VINS or LiDAR-Inertial Navigation System (LINS) and does not require any precise initial robot pose, refining the initial pose estimation during robot navigation.

Future work is to test this methodology on other LVS typologies, such as visual odometry extracted from event cameras [12], [13] in an Intervention-AUV application. Also, it is interesting to test the robustness on the IMU bias estimation provided by the LVS preintegration for lower-grade IMUs. Moreover, develop a methodology to update the preintegrated measurements depending on the LVS level arm it would allow its calibration and improve the robot navigation. An interesting research question is if it is possible to extend the Special Galilean Group $SGal(3)$ [39] in N isometries in the same way that we extended the $SE(3)$ group. By using this group, time is also contained within the group, modeling not only the problem geometry, but also the physics. Thus, the automorphism of the preintegration model in (12) is no longer necessary and Υ and Γ elements can be deduced directly from the exponential function definition, without the need to impose any assumptions. Finally, the proposed preintegration framework could be applied in a Graph SLAM problem, for instance to build a Multibeam ecosounder Inertial Navigation System (MINS) applying sonar scan matching.

APPENDIX

Proposition 1: Given a pose $T \in SE_2(3)$ and $\Phi_{SE_2(3)} : SE_2(3), \mathbb{R} \rightarrow SE_2(3)$ defined as

$$\Phi_{SE_2(3)}(T, \tau) = \left[\begin{array}{c|c} R & p + \tau v \\ \hline 0_{2 \times 3} & I_2 \end{array} \right] \quad (44)$$

then

$$F_{SE_2(3)}(\tau) = \frac{\partial \Phi_{SE_2(3)}(T, \tau)}{\partial T} = \left[\begin{array}{ccc} I_3 & 0_3 & 0_3 \\ 0_3 & I_3 & \tau I_3 \\ 0_3 & 0_3 & I_3 \end{array} \right]. \quad (45)$$

Proof: Applying the derivative definition

$$\frac{\partial \Phi(T)}{\partial T} = \lim_{\varepsilon \rightarrow 0} \frac{\Phi(T \oplus \varepsilon) \ominus \Phi(T)}{\varepsilon} \quad (46)$$

where $\varepsilon = [\phi^T \ \rho^T \ \nu^T]^T$ is a perturbation defined at the tangent space of T . Developing terms we arrive at

$$\Phi(T \oplus \varepsilon) = \Phi(T \cdot \text{Exp}(\varepsilon)) = \left[\begin{array}{c|c} \text{Rexp}(\phi) & a \mid b \\ \hline 0_{2 \times 3} & I_2 \end{array} \right] \quad (47)$$

where $a = RJ_l(\phi)(\rho + \nu\tau) + p + v\tau$, $b = RJ_l(\phi)\nu + v$ and

$$\Phi(T)^{-1} = \left[\begin{array}{c|c} R^T & -R^T(p + \tau v) \mid -R^T v \\ \hline 0_{2 \times 3} & I_2 \end{array} \right]. \quad (48)$$

Composing (47) and (48), we get

$$\begin{aligned} \Phi(T \oplus \varepsilon) \ominus \Phi(T) &= \text{Log} [\Phi(T)^{-1} \cdot \Phi(T \oplus \varepsilon)] \\ &= \left[\begin{array}{ccc} I_3 & 0_3 & 0_3 \\ 0_3 & I_3 & \tau I_3 \\ 0_3 & 0_3 & I_3 \end{array} \right] \begin{bmatrix} \phi \\ \rho \\ \nu \end{bmatrix}. \end{aligned} \quad (49)$$

Substituting back (49) to the definition in (46), we obtain

$$\frac{\partial \Phi(T)}{\partial T} = \lim_{\varepsilon \rightarrow 0} \left[\begin{array}{ccc} I_3 & 0_3 & 0_3 \\ 0_3 & I_3 & \tau I_3 \\ 0_3 & 0_3 & I_3 \end{array} \right] = \left[\begin{array}{ccc} I_3 & 0_3 & 0_3 \\ 0_3 & I_3 & \tau I_3 \\ 0_3 & 0_3 & I_3 \end{array} \right]. \quad (50)$$

Proposition 2: Given a pose $T \in SE_3(3)$ and $\Phi_{SE_3(3)} : SE_3(3), \mathbb{R} \rightarrow SE_3(3)$ defined as

$$\Phi_{SE_3(3)}(T, \tau) = \left[\begin{array}{c|c} R & p + \tau v \mid v \mid p \\ \hline 0_3 & I_3 \end{array} \right] \quad (51)$$

then

$$F_{SE_3(3)}(\tau) = \frac{\partial \Phi_{SE_3(3)}(T, \tau)}{\partial T} = \left[\begin{array}{cccc} I_3 & 0_3 & 0_3 & 0_3 \\ 0_3 & I_3 & \tau I_3 & 0_3 \\ 0_3 & 0_3 & I_3 & 0_3 \\ 0_3 & 0_3 & 0_3 & I_3 \end{array} \right]. \quad (52)$$

Proof: Applying the derivative definition in (46) and following a development similar to (47) and (48) we get:

$$\Phi(T \oplus \varepsilon) \ominus \Phi(T) = \text{Log} [\Phi(T)^{-1} \cdot \Phi(T \cdot \text{Exp}(\varepsilon))]$$

$$= \left[\begin{array}{cccc} I_3 & 0_3 & 0_3 & 0_3 \\ 0_3 & I_3 & \tau I_3 & 0_3 \\ 0_3 & 0_3 & I_3 & 0_3 \\ 0_3 & 0_3 & 0_3 & I_3 \end{array} \right] \begin{bmatrix} \phi \\ \rho \\ \nu \\ \rho \end{bmatrix}. \quad (53)$$

Substituting back (53) to the definition in (46), we obtain

$$\frac{\partial \Phi(T)}{\partial T} = \lim_{\varepsilon \rightarrow 0} \left[\begin{array}{cccc} I_3 & 0_3 & 0_3 & 0_3 \\ 0_3 & I_3 & \tau I_3 & 0_3 \\ 0_3 & 0_3 & I_3 & 0_3 \\ 0_3 & 0_3 & 0_3 & I_3 \end{array} \right] = \left[\begin{array}{cccc} I_3 & 0_3 & 0_3 & 0_3 \\ 0_3 & I_3 & \tau I_3 & 0_3 \\ 0_3 & 0_3 & I_3 & 0_3 \\ 0_3 & 0_3 & 0_3 & I_3 \end{array} \right]. \quad (54)$$

Proposition 3: Given a pose $T \in SE_2(3)$ and $\mu_{SE_3(3)} : SE_2(3) \rightarrow SE_3(3)$ defined as

$$\mu_{SE_3(3)}(T) = \left[\begin{array}{c|c} R & p \mid v \mid p \\ \hline 0_3 & I_3 \end{array} \right] \quad (55)$$

then

$$M_{SE_3(3)} = \frac{\partial \mu_{SE_3(3)}(T)}{\partial T} = \left[\begin{array}{ccc} I_3 & 0_3 & 0_3 \\ 0_3 & I_3 & 0_3 \\ 0_3 & 0_3 & I_3 \\ 0_3 & I_3 & 0_3 \end{array} \right]. \quad (56)$$

Proof: Applying the derivative definition

$$\frac{\partial \mu(T)}{\partial T} = \lim_{\varepsilon \rightarrow 0} \frac{\mu(T \oplus_{SE_2(3)} \varepsilon) \ominus_{SE_3(3)} \mu(T)}{\varepsilon} \quad (57)$$

where $\varepsilon = [\phi^T \ \rho^T \ \nu^T]^T$ is a perturbation defined at the tangent space of T . Following a development similar to (47) and (48), we get

$$\begin{aligned} \mu(T \oplus \varepsilon) \ominus \mu(T) &= \text{Log} [\mu(T)^{-1} \cdot \mu(T \cdot \text{Exp}(\varepsilon))] \\ &= \left[\begin{array}{ccc} I_3 & 0_3 & 0_3 \\ 0_3 & I_3 & 0_3 \\ 0_3 & 0_3 & I_3 \\ 0_3 & I_3 & 0_3 \end{array} \right] \begin{bmatrix} \phi \\ \rho \\ \nu \end{bmatrix}. \end{aligned} \quad (58)$$

Substituting back (58) to the definition in (57), we obtain

$$\frac{\partial \mu(T)}{\partial T} = \lim_{\varepsilon \rightarrow 0} \left[\begin{array}{ccc} I_3 & 0_3 & 0_3 \\ 0_3 & I_3 & 0_3 \\ 0_3 & 0_3 & I_3 \\ 0_3 & I_3 & 0_3 \end{array} \right] = \left[\begin{array}{ccc} I_3 & 0_3 & 0_3 \\ 0_3 & I_3 & 0_3 \\ 0_3 & 0_3 & I_3 \\ 0_3 & I_3 & 0_3 \end{array} \right]. \quad (59)$$

Proposition 4: Given a pose $T \in SE_2(3)$ and $\psi_{SE_2(3)} : SE_2(3) \rightarrow SE_2(3)$ defined as

$$\psi_{SE_2(3)}(T) = \left[\begin{array}{c|c} R & p \mid v + [\Omega]_{\times} p \\ \hline 0_{2 \times 3} & I_2 \end{array} \right] \quad (60)$$

then

$$\Psi_{SE_2(3)}(T) = \frac{\partial \psi_{SE_2(3)}(T)}{\partial T} = \left[\begin{array}{ccc} I_3 & 0_3 & 0_3 \\ 0_3 & I_3 & 0_3 \\ 0_3 & [R^T \Omega]_{\times} & I_3 \end{array} \right]. \quad (61)$$

Proof: Applying the derivative definition

$$\frac{\partial \psi(T)}{\partial T} = \lim_{\varepsilon \rightarrow 0} \frac{\psi(T \oplus \varepsilon) \ominus \psi(T)}{\varepsilon} \quad (62)$$

where $\varepsilon = [\phi \ \rho \ \nu]^T$ is a perturbation defined at the tangent space of T . Developing terms we arrive at

$$\psi(T \oplus \varepsilon) = \psi(T \cdot \text{Exp}(\varepsilon)) = \left[\begin{array}{c|c} \text{Rexp}(\phi) & a \ | \ b \\ \hline 0_{2 \times 3} & I_2 \end{array} \right] \quad (63)$$

where $a = RJ_l(\phi)\rho + p$, $b = RJ_l(\phi)\nu + v + [\Omega]_{\times}(RJ_l(\phi)\rho + p)$

$$\psi(T)^{-1} = \left[\begin{array}{c|c} R^T & -R^T p \ | \ -R^T(v + [\Omega]_{\times} p) \\ \hline 0_{2 \times 3} & I_2 \end{array} \right]. \quad (64)$$

Composing (63) and (64), we get

$$\begin{aligned} \psi(T \oplus \varepsilon) \ominus \psi(T) &= \text{Log} [\psi(T)^{-1} \cdot \psi(T \oplus \varepsilon)] \\ &= \left[\begin{array}{ccc} I_3 & 0_3 & 0_3 \\ 0_3 & I_3 & 0_3 \\ 0_3 & C & I_3 \end{array} \right] \left[\begin{array}{c} \phi \\ \rho \\ \nu \end{array} \right] \end{aligned} \quad (65)$$

where $C = J_l^{-1}(\phi)[R^T \Omega]_{\times} J_l(\phi)$. Considering that for small rotations $J_l(\phi) \approx I_3 + \frac{1}{2}[\phi]_{\times}$ and $J_l^{-1}(\phi) \approx I_3 - \frac{1}{2}[\phi]_{\times}$

$$\lim_{\phi \rightarrow 0} J_l^{-1}(\phi)[R^T \Omega]_{\times} J_l(\phi) = [R^T \Omega]_{\times} \quad (66)$$

Substituting back (65) to the definition in (62) considering (66), we obtain

$$\frac{\partial \psi(T)}{\partial T} = \lim_{\varepsilon \rightarrow 0} \left[\begin{array}{ccc} I_3 & 0_3 & 0_3 \\ 0_3 & I_3 & 0_3 \\ 0_3 & C & I_3 \end{array} \right] = \left[\begin{array}{ccc} I_3 & 0_3 & 0_3 \\ 0_3 & I_3 & 0_3 \\ 0_3 & [R^T \Omega]_{\times} & I_3 \end{array} \right]. \quad (67)$$

Proposition 5: Given a pose $T \in SE_3(3)$ and $\psi_{SE_3(3)} : SE_3(3) \rightarrow SE_3(3)$ defined as

$$\psi_{SE_3(3)}(T) = \left[\begin{array}{c|c} R \ | \ p_1 \ | \ v + [\Omega]_{\times} p_1 \ | \ p_2 \\ \hline 0_3 \ | \ I_3 \end{array} \right] \quad (68)$$

then

$$\Psi_{SE_3(3)}(T) = \frac{\partial \psi_{SE_3(3)}(T)}{\partial T} = \left[\begin{array}{ccc} I_3 & 0_3 & 0_3 & 0_3 \\ 0_3 & I_3 & 0_3 & 0_3 \\ 0_3 & [R^T \Omega]_{\times} & I_3 & 0_3 \\ 0_3 & 0_3 & 0_3 & I_3 \end{array} \right]. \quad (69)$$

Proof: Applying the derivative definition in (62) and following a development similar to (63) and (64), we get

$$\begin{aligned} \psi(T \oplus \varepsilon) \ominus \psi(T) &= \text{Log} [\psi(T)^{-1} \cdot \psi(T \cdot \text{Exp}(\varepsilon))] \\ &= \left[\begin{array}{ccc} I_3 & 0_3 & 0_3 & 0_3 \\ 0_3 & I_3 & 0_3 & 0_3 \\ 0_3 & C & I_3 & 0_3 \\ 0_3 & 0_3 & 0_3 & I_3 \end{array} \right] \left[\begin{array}{c} \phi \\ \rho \\ \nu \end{array} \right] \end{aligned} \quad (70)$$

where C is defined in (65). Substituting back (70) to the definition in (62) considering (66), we obtain

$$\begin{aligned} \frac{\partial \psi(T)}{\partial T} &= \lim_{\varepsilon \rightarrow 0} \left[\begin{array}{ccc} I_3 & 0_3 & 0_3 & 0_3 \\ 0_3 & I_3 & 0_3 & 0_3 \\ 0_3 & C & I_3 & 0_3 \\ 0_3 & 0_3 & 0_3 & I_3 \end{array} \right] \\ &= \left[\begin{array}{ccc} I_3 & 0_3 & 0_3 & 0_3 \\ 0_3 & I_3 & 0_3 & 0_3 \\ 0_3 & [R^T \Omega]_{\times} & I_3 & 0_3 \\ 0_3 & 0_3 & 0_3 & I_3 \end{array} \right]. \end{aligned} \quad (71)$$

REFERENCES

- [1] F. Dellaert and M. Kaess, *Factor Graphs for Robot Perception*. Boston, MA, USA: Now, 2017.
- [2] T. Lupton and S. Sukkarieh, "Visual-inertial-aided navigation for high-dynamic motion in build environments without initial conditions," *IEEE Trans. Robot.*, vol. 28, no. 1, pp. 61–76, Feb. 2012.
- [3] C. Foster, L. Carlone, F. Dellaert, and D. Scaramuzza, "On-manifold preintegration for real-time visual-inertial odometry," *IEEE Trans. Robot.*, vol. 33, no. 1, pp. 1–21, Feb. 2017.
- [4] T. Qin, P. Li, and S. Shen, "VINS-mono: A robust and versatile monocular visual-inertial state estimator," *IEEE Trans. Robot.*, vol. 34, no. 4, pp. 1004–1020, Aug. 2018.
- [5] T. Shan, B. Englot, D. Meyers, W. Wang, C. Ratti, and D. Rus, "LIO-SAM: Tightly-coupled lidar inertial odometry via smoothing and mapping," in *Proc. IEEE/RSJ Int. Conf. Intell. Robots Syst.*, 2020, pp. 5135–5142.
- [6] W. Wen, T. Pfeifer, X. Bai, and L. Hsu, "Factor graph optimization for GNSS/INS integration: A comparison with the extended Kalman filter," *J. Inst. Navigation*, vol. 68, no. 2, pp. 315–331, 2021.
- [7] D. Wisth, M. Camurri, and M. Fallon, "VILENS: Visual, inertial, Lidar, and leg odometry for all-terrain legged robots," *IEEE Trans. Robot.*, vol. 39, no. 1, pp. 309–326, Feb. 2023.
- [8] A. Thoms, G. Earle, N. Charron, and S. Narasimhan, "Tightly coupled, graph-based DVL/IMU fusion and decoupled mapping for SLAM-centric maritime infrastructure inspection," *IEEE J. Ocean. Eng.*, vol. 48, no. 3, pp. 663–676, Jul. 2023.
- [9] J. Wang, L. Li, H. Yu, X. Gui, and Z. Li, "VIMO: A visual-inertial-magnetic navigation system based on non-linear optimization," *Sensors*, vol. 20, no. 16, 2020, Art. no. 4386.
- [10] M. Kimishima, T. Sawada, A. Sonoura, T. Amano, H. Kamata, and K. Yamashita, "Highly accurate inertial navigation that compensates for the earth's rotation and sensor bias using non-holonomic constraints," in *Proc. 2023 IEEE Int. Symp. Inertial Sensors Syst.*, 2023, pp. 1–4.
- [11] B. M. Sun, H. K. Russell, M. B. Yearly, H. H. Sigmarsson, and J. W. McDaniel, "Reduced navigation error using a multi-sensor fusion technique and its application in synthetic aperture radar," *IEEE J. Microw.*, vol. 4, no. 1, pp. 86–100, Jan. 2024.
- [12] A. Z. Zhu, L. Yuan, K. Chaney, and K. Daniilidis, "Unsupervised event-based learning of optical flow, depth, and egomotion," in *Proc. IEEE/CVF Conf. Comput. Vis. Pattern Recognit.*, 2019, pp. 989–997.
- [13] Y. Tian and J. Andrade-Cetto, "Egomotion from event-based SNN optical flow," in *Proc. 2023 Int. Conf. Neuromorphic Syst.*, 2023, pp. 1–8.
- [14] M. Fourmy, T. Flayols, P.-A. Léziart, N. Mansard, and J. Solà, "Contact forces preintegration for estimation in legged robotics using factor graphs," in *Proc. IEEE Int. Conf. Robot. Automat.*, 2021, pp. 1372–1378.
- [15] J. Martí Suamell, "Agile aerial manipulation: An approach based on full-body dynamics and model predictive control," PhD thesis, Universitat Politècnica de Catalunya, 2024, *confidential document*.
- [16] J. Solà, J. Deray, and D. Atchuthan, "A micro lie theory for state estimation in robotics," 2020, *arXiv:1812.01537*.
- [17] T. Lupton and S. Sukkarieh, "Efficient integration of inertial observations into visual slam without initialization," in *Proc. IEEE/RSJ Int. Conf. Intell. Robots Syst.*, 2009, pp. 1547–1552.
- [18] V. Indelman, S. Williams, M. Kaess, and F. Dellaert, "Information fusion in navigation systems via factor graph based incremental smoothing," *Robot. Auton. Syst.*, vol. 61, no. 8, pp. 721–738, 2013.

- [19] C. Foster, L. Carlone, F. Dellaert, and D. Scaramuzza, "IMU preintegration on manifold for efficient visual-inertial maximum-a-posteriori estimation," *Robot.: Sci. Syst. XI*, Rome, 2015.
- [20] F. Dellaert, "Gtsam 4.0: Factor graphs for sensor fusion in robotics," [Online]. Available: <https://gtsam.org/>
- [21] K. Eickenhoff, P. Geneva, and G. Huang, "Direct visual-inertial navigation with analytical preintegration," in *Proc. IEEE Int. Conf. Robot. Automat.*, 2017, pp. 1429–1435.
- [22] K. Eickenhoff, P. Geneva, and G. Huang, "Closed-form preintegration methods for graph-based visual-inertial navigation," *Int. J. Robot. Res.*, vol. 38, no. 5, pp. 563–586, 2019.
- [23] A. Barrau and S. Bonnabel, "A mathematical framework for IMU error propagation with applications to preintegration," in *Proc. 2020 IEEE Int. Conf. Robot. Automat.*, 2020, pp. 5732–5738.
- [24] M. Brossard, A. Barrau, P. Chauchat, and S. Bonnabel, "Associating uncertainty to extended poses for on lie group IMU preintegration with rotating earth," *IEEE Trans. Robot.*, vol. 38, no. 2, pp. 998–1015, Apr. 2022.
- [25] H. Tang, T. Zhang, X. Niu, J. Fan, and J. Liu, "Impact of the earth rotation compensation on MEMS-IMU preintegration of factor graph optimization," *IEEE Sensors J.*, vol. 22, no. 17, pp. 17194–17204, Sep. 2022.
- [26] J. Jiang, X. Niu, and J. Liu, "Improved imu preintegration with gravity change and earth rotation for optimization-based GNSS/VINS," *Remote Sens.*, vol. 12, no. 18, 2020, Art. no. 3048.
- [27] L. Zhang, W. Wen, L. Hsu, and T. Zhang, "An improved inertial preintegration model in factor graph optimization for high accuracy positioning of intelligent vehicles," *IEEE Trans. Intell. Veh.*, vol. 9, no. 1, pp. 1641–1653, Jan. 2024.
- [28] J. Ding, C. Huang, J. Cheng, F. Wang, and Y. Hu, "Refined on-manifold imu preintegration theory for factor graph optimization based on equivalent rotation vector," *IEEE Sensors J.*, vol. 23, no. 5, pp. 5200–5219, Mar. 2023.
- [29] L. Chang, X. Niu, and T. Liu, "GNSS/IMU/ODO/LiDAR-SLAM integrated navigation system using IMU/ODO pre-integration," *Sensors*, vol. 20, no. 17, 2020, Art. no. 4702.
- [30] S. Bai, J. Lai, P. Lyu, Y. Cen, and B. Ji, "Improved preintegration method for GNSS/IMU/in-vehicle sensors navigation using graph optimization," *IEEE Trans. Veh. Technol.*, vol. 70, no. 11, pp. 11446–11457, Nov. 2021.
- [31] R. Buchanan, V. Agrawal, M. Camurri, F. Dellaert, and M. Fallon, "Deep IMU bias inference for robust visual-inertial odometry with factor graphs," *IEEE Robot. Automat. Lett.*, vol. 8, no. 1, pp. 41–48, Jan. 2023.
- [32] C. L. Gentil and T. Vidal-Calleja, "Continuous latent state preintegration for inertial-aided systems," *Int. J. Robot. Res.*, vol. 42, no. 10, pp. 874–900, 2023.
- [33] A. Barrau and S. Bonnabel, "An EKF-SLAM algorithm with consistency properties," 2015, *arXiv:1510.06263*.
- [34] X. Li, H. Jiang, X. Chen, H. Kong, and J. Wu, "Closed-form error propagation on $se_n(3)$ group for invariant EKF with applications to VINS," *IEEE Robot. Automat. Lett.*, vol. 7, no. 4, pp. 10705–10712, Oct. 2022.
- [35] A. Barrau and S. Bonnabel, "Linear observed systems on groups," *Syst. Control Lett.*, vol. 129, pp. 36–42, 2019.
- [36] P. Vial, M. Castellón, N. Palomerias, M. Carreras, and P. Ridao, "Inertial navigation framework for multimodal underwater graph SLAM," in *Proc. IEEE OCEANS 2023-Limerick*, 2023, pp. 1–8.
- [37] M. Kaess, H. Johannsson, R. Roberts, V. Ila, J. Leonard, and F. Dellaert, "ISAM2: Incremental smoothing and mapping using the Bayes tree," *Int. J. Robot. Res.*, vol. 31, pp. 216–235, 2012.
- [38] D. Ribas, N. Palomerias, P. Ridao, M. Carreras, and A. Mallios, "Girona 500 AUV: From survey to intervention," *IEEE/ASME Trans. Mechatron.*, vol. 17, no. 1, pp. 46–53, Feb. 2012.
- [39] J. Kelly, "All about the Galilean group SGAL(3)," 2023, *arXiv:2312.07555*.



Pau Vial received the B.S. degree in industrial engineering from Universitat de Girona, Catalunya, Spain, in 2018 (where he also received the best Bachelor student award) and the M.Sc. degree in industrial engineering from the Universitat Politècnica de Catalunya, Catalunya, in 2020. He is currently working toward the Ph.D. degree in localization techniques for an AUV with the Institut VICOROB from the Universitat de Girona.

His research interests include optimization techniques, machine learning and Lie theory applied to underwater robotic navigation.



Joan Solà received the M.Sc. degree in telecommunication and electronics from the Universitat Politècnica de Catalunya, Catalunya, Spain, and the Ph.D. degree in robotics from the University of Toulouse, Toulouse, France, in 2007.

He is currently a CSIC Researcher with the Institut de Robòtica i Informàtica Industrial, Barcelona. He has contributed to monocular SLAM and is interested in state estimation for robots with particularly large dynamics and degrees of freedom, such as humanoids and aerial manipulators. His current projects

turn around whole-body estimation and control, including multisensor fusion, SLAM, machine learning, and model predictive control.



Narcís Palomerias received the B.Sc. degree in computer science and the Ph.D. degree in computer engineering from the Universitat de Girona, Catalunya, Spain, in 2004 and 2011, respectively.

He is a Postdoctoral Fellow with the Institut VICOROB. He has participated in several international research projects and his activity is mainly focused on underwater robotics in topics like intelligent control architectures and mission control.



Marc Carreras (Member, IEEE) received the B.Sc. degree in industrial engineering and the Ph.D. degree in computer engineering from the Universitat de Girona, Catalunya, Spain, in 1998 and 2003, respectively.

He has participated in 18 research projects, he is author of more than 90 publications, he has supervised six Ph.D. thesis and he has won several international AUV competitions. He is an Associate Professor with the Institut VICOROB. His activity is mainly focused on underwater robotics in topics like intelligent control architectures, robot learning, and path planning.